# Journal Pre-proof


Design, synthesis and biological evaluation of novel vicinal diaryl-substituted 1*H*-Pyrazole analogues of combretastatin A-4 as highly potent tubulin polymerization inhibitors

Romeo Romagnoli, Paola Oliva, Maria Kimatrai Salvador, Maria Encarnacion Camacho, Chiara Padroni, Andrea Brancale, Salvatore Ferla, Ernest Hamel, Roberto Ronca, Elisabetta Grillo, Roberta Bortolozzi, Fatlum Rruga, Elena Mariotto, Giampietro Viola

PII: S0223-5234(19)30707-X

DOI: https://doi.org/10.1016/j.ejmech.2019.111577

Reference: EJMECH 111577

To appear in: *European Journal of Medicinal Chemistry*

Received Date: 26 June 2019

Revised Date: 30 July 2019

Accepted Date: 30 July 2019

Please cite this article as: R. Romagnoli, P. Oliva, M.K. Salvador, M.E. Camacho, C. Padroni, A. Brancale, S. Ferla, E. Hamel, R. Ronca, E. Grillo, R. Bortolozzi, F. Rruga, E. Mariotto, G. Viola, Design, synthesis and biological evaluation of novel vicinal diaryl-substituted 1*H*-Pyrazole analogues of combretastatin A-4 as highly potent tubulin polymerization inhibitors, *European Journal of Medicinal Chemistry* (2019), doi: https://doi.org/10.1016/j.ejmech.2019.111577.

# Design, Synthesis and Biological Evaluation of Novel Vicinal Diaryl-Substituted 1*H*-Pyrazole Analogues of Combretastatin A-4 as Highly Potent Tubulin Polymerization Inhibitors

Romeo Romagnoli,[a]* Paola Oliva,[a] Maria Kimatrai Salvador,[b] Maria Encarnacion Camacho,[b] Chiara Padroni,[c] Andrea Brancale,[d] Salvatore Ferla,[d] Ernest Hamel,[e] Roberto Ronca,[f] Elisabetta Grillo,[f] Roberta Bortolozzi,[g] Fatlum Rruga,[g] Elena Mariotto[g] and Giampietro Viola[g,h]*

[a]Dipartimento di Scienze Chimiche e Farmaceutiche, Università di Ferrara, Ferrara, Italy; [b]Departamento de Química Farmacéutica y Orgánica, Facultad de Farmacia, Granada, Spain; [c]Aptuit, an Evotec Company, Verona, Italy; [d]School of Pharmacy and Pharmaceutical Sciences, Cardiff University, Cardiff, UK; [e]National Cancer Institute, National Institutes of Health, Frederick, Maryland USA; [f]Dipartimento di Medicina Molecolare e Traslazionale Università di Brescia, Brescia, Italy; [g]Dipartimento di Salute della Donna e del Bambino, Università di Padova, Padova, Italy; [h]Istituto di Ricerca Pediatrica (IRP), Padova, Italy

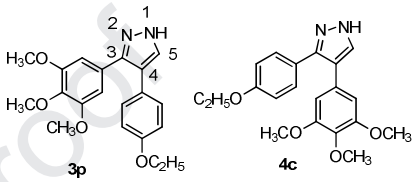


$IC_{50}$: 0.06-3.2 nM as antiproliferative agent
$IC_{50}$: 0.36 μM as inhibitor of tubulin polymerization

Comparing couple of regioisomeric derivatives **3p** and **4c** there was not substantial difference of antiproliferative as well as of tubulin polymerization inhibitory activity between 3',4',5'-trimethoxyphenyl moiety located at the 3- or 4-position of the pyrazole ring.

# Design, Synthesis and Biological Evaluation of Novel Vicinal Diaryl-Substituted 1*H*-Pyrazole Analogues of Combretastatin A-4 as Highly Potent Tubulin Polymerization Inhibitors

Romeo Romagnoli,[a]* Paola Oliva,[a] Maria Kimatrai Salvador,[b] Maria Encarnacion Camacho,[b] Chiara Padroni,[c] Andrea Brancale,[d] Salvatore Ferla,[d] Ernest Hamel,[e] Roberto Ronca,[f] Elisabetta Grillo,[f] Roberta Bortolozzi,[g] Fatlum Rruga,[g] Elena Mariotto[g] and Giampietro Viola[g,h]*

[a]Dipartimento di Scienze Chimiche e Farmaceutiche, Via Luigi Borsari 46, Università di Ferrara, 44121 Ferrara, Italy;

[b]Departamento de Química Farmacéutica y Orgánica, Facultad de Farmacia, Campus de Cartuja s/n, 18071, Granada, Spain;

[c]Aptuit, an Evotec Company, Via A. Fleming 4, 37135 Verona, Italy;

[d]School of Pharmacy and Pharmaceutical Sciences, Cardiff University, King Edward VII Avenue, Cardiff, CF10 3NB, UK;

[e]Screening Technologies Branch, Developmental Therapeutics Program, Division of Cancer Treatment and Diagnosis, Frederick National Laboratory for Cancer Research, National Cancer Institute, National Institutes of Health, Frederick, Maryland 21702, USA;

[f]Dipartimento di Medicina Molecolare e Traslazionale Unità di Oncologia Sperimentale ed Immunologia, Università di Brescia, 25123 Brescia, Italy;

[g]Dipartimento di Salute della Donna e del Bambino, Laboratorio di Oncoematologia, Università di Padova, 35131 Padova, Italy

[h]Istituto di Ricerca Pediatrica (IRP), Corso Stati Uniti 4, 35128 Padova, Italy

*To whom correspondence should be addressed. E-mail: rmr@unife.it; Phone: 39-(0)532-455303. Fax: 39-(0)532-455953. (R.R.); E-mail: giampietro.viola.1@unipd.it Phone: 39-(0)49-8215485. Fax: 39-(0)49-8211462. (G.V.).

**Abstract:** A series of 3-(3',4',5'-trimethoxyphenyl)-4-substituted 1*H*-pyrazole and their related 3-aryl-4-(3',4',5'-trimethoxyphenyl)-1-*H*-pyrazole regioisomeric derivatives, prepared as *cis*-rigidified combretastatin A-4 (CA-4) analogues, were synthesized and evaluated for their *in vitro* antiproliferative against six different cancer cell lines and, for selected highly active compounds, inhibitory effects on tubulin polymerization, cell cycle effects and *in vivo* potency. We retained the 3',4',5'-trimethoxyphenyl moiety as ring A throughout the present investigation, and a structure-activity relationship (SAR) information was obtained by adding electron-withdrawing ($OCF_3$, $CF_3$) or electron-releasing (alkyl and alkoxy) groups on the second aryl ring, corresponding to the B-ring of CA-4, either at the 3- or 4-position of the pyrazole nucleus. In addition, the B-ring was replaced with a benzo[*b*]thien-2-yl moiety. For many of the compounds, their activity was greater than, or comparable with, that of CA-4. Maximal activity was observed with the two regioisomeric derivatives characterized by the presence of a 4-ethoxyphenyl and a 3',4',5'-trimethoxyphenyl group at the C-3 and C-4 positions, and vice versa, of the 1*H*-pyrazole ring. The data showed that the 3',4',5'-trimethoxyphenyl moiety can be moved from the 3- to the 4-position of the 1*H*-pyrazole ring without significantly affecting antiproliferative activity. The most active derivatives bound to the colchicine site of tubulin and inhibited tubulin polymerization at submicromolar concentrations. In vivo experiments, on an orthotopic murine mammary tumor, revealed that 4c inhibited tumor growth even at low concentrations (5 mg/kg) compared to CA-4P (30 mg/kg).

**Keywords.** Microtubules, structure-activity relationship, 1*H*-pyrazole, antiproliferative activity, tubulin.

## 1. Introduction

Microtubules are cylindrical structures formed by a polymerization process from αβ-tubulin heterodimers and are dynamic components of the cytoskeleton of eukaryotic cells. Their dynamic functions include the formation and disappearance of the mitotic spindle, which is required for the separation of duplicated chromosomes during cell division [1]. The microtubule system is involved in a number of other cellular functions as well, including determination and maintenance of cell shape, organization of intracellular architecture, secretion, cellular transport, regulation of motility and intracellular organelle transport [2].

Therefore, especially since tubulin is a validated target for drugs active against cancer, there has been great interest in identifying and developing new tubulin polymerization inhibitors. Inhibition of microtubule function using agents that interact specifically with tubulin, many of which are natural products, remains one approach for the development of new cytotoxic anticancer drugs [3]. Among the naturally occurring antimitotic agents, combretastatin A-4 (CA-4, **1a**; Figure 1), isolated from the bark of the South African tree *Combretum caffrum* [4], is one of the best known inhibitors of tubulin assembly. CA-4 affects microtubule dynamics by interacting with tubulin at the colchicine site [5]. CA-4 shows potent cytotoxicity against a wide variety of human cancer cell lines, including those that are multidrug resistant [6]. Due to the low water solubility of CA-4, the corresponding disodium phosphate salt (CA-4P, **1b**) was synthesized as a water soluble pro-drug. CA-4P causes rapid and selective vascular shutdown of the blood vessels of tumors, consistent with an anti-vascular mechanism of action as a vascular disrupting agent (VDA), and CA-4P has shown promising results in phase II and III clinical trials on advanced and solid tumors [7].

The activity and structural simplicity of CA-4 have stimulated significant interest in the development of a wide variety of analogues that mimic the pharmacological properties of CA-4. These analogues include compounds modified in ring A, ring B and the ethylene bridge [8]. Previous structure-activity relationship (SAR) studies have demonstrated that both the 3',4',5'-trimethoxy substitution pattern on the A-ring and the *cis*-orientation of the vinyl bond were essential for optimal antiproliferative activity. B-ring structural modifications were tolerated by the target, with the 3'-hydroxy group not necessary for potent activity while the 4'-methoxy group was crucial for cytoxicity [9].

However, several studies have established that the *cis*-olefinic double bond of CA-4 tends to isomerize to the thermodynamically more stable *trans*-form during storage and in the course of metabolism in liver microsomes, resulting in a dramatic decrease in both antitubulin and antiproliferative activities.

Thus, with the aim of retaining the *cis*-olefin configuration of CA-4 required for bioactivity, a strategy to overcome the problem of *cis* to *trans* isomerization developed in which the ethylene bridge was incorporated into 1,2-diaryl-substituted five-membered aromatic heterocyclic rings, which can be considered as non-isomerizable and chemically stable *Z*-restricted isosteres of CA-4 [10].

In the designed analogues, several research groups have developed a number of compounds containing pyrazole as the surrogate of the stilbene core of CA-4 and that maintain the structural elements of CA-4, such as the presence of 3',4',5'-trimethoxyphenyl A-ring, which was considered to be fundamental for the tubulin binding activity, whereas variations were made in the vicinal substituent, corresponding to B-ring of CA-4.

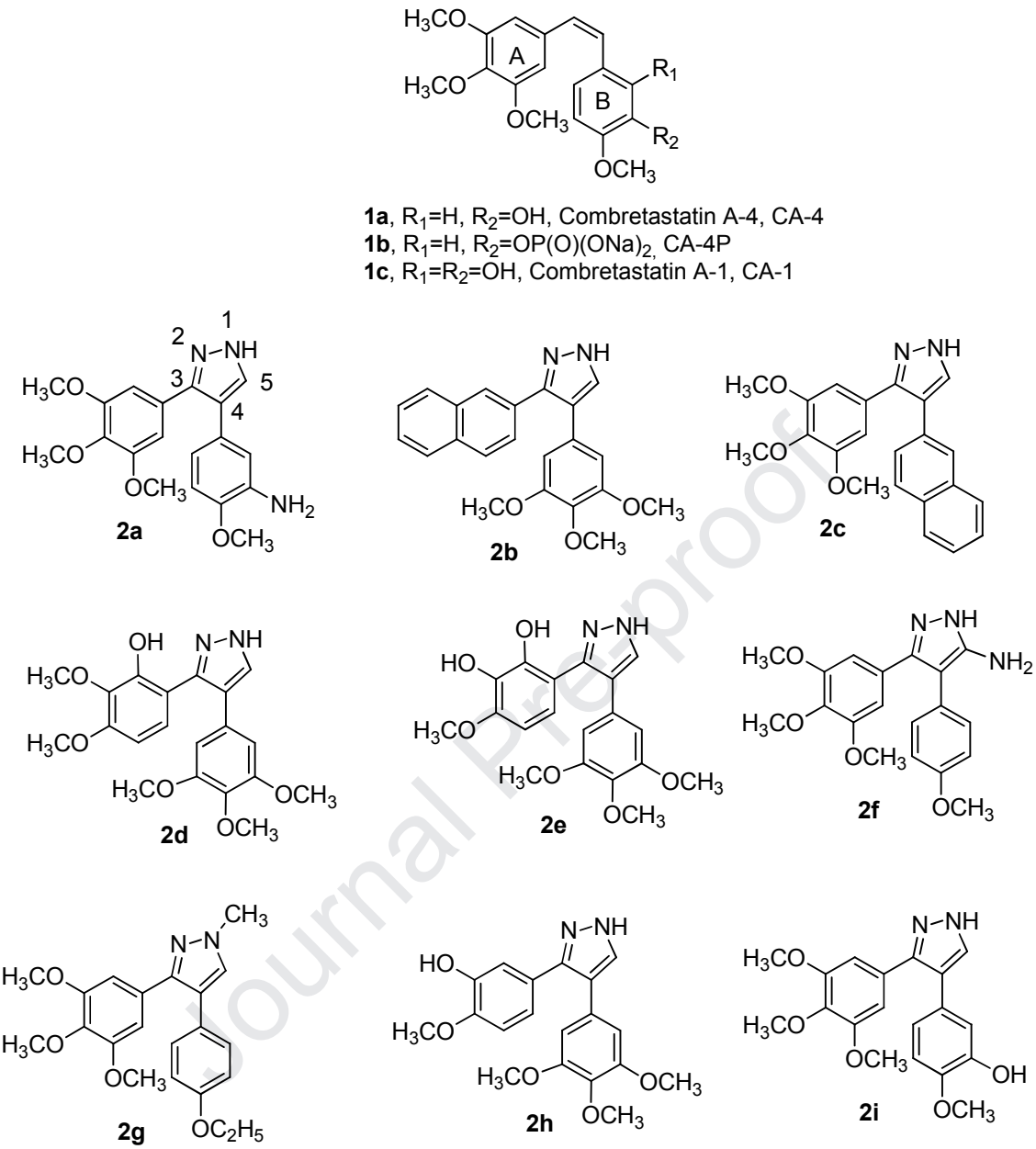


**Figure 1**. Structures of CA-4 (**1a**), CA-4P (**1b**) and CA-1 (**1c**) and molecular formulas of several synthesized 3,4-disubstituted 1*H*-pyrazoles (**2a-i**) previously reported in the literature.

As far as pyrazole derivatives are concerned, Ohsumi et al. reported the preparation of 3-(3',4',5'-trimethoxyphenyl)-4-(3'-amino-4'-methoxyphenyl)-1*H*-pyraziole **2a**, which showed potent antimitotic activity in the tubulin polymerization assay, with an $IC_{50}$ value of 3 μM. Compound **2a** was also a potent antiproliferative agent ($IC_{50}$: 8.4 nM)

against the colon-26 adenocarcinoma cell line [11]. In a previous study, Medarde and co-workers also described two 3,4-disubstituted pyrazole derivatives (**2b** and **2c**), obtained by reversing the positions of the 2'-naphthyl and 3',4',5'-trimethoxyphenyl ring moieties. Both these compounds showed potent antiproliferative activity against HCT-116 (human colon carcinoma) and A549 (human lung adenocarcinoma) cancer cell lines, with $IC_{50}$ values ranging from 6 to 37 nM. Both these compounds had 10-fold reduced activity relative to that of CA-4 as inhibitors of tubulin polymerization [12]. Pirali and co-workers also reported a concise synthesis of 3,4-diarylpyrazole derivatives as rigidified analogues of CA-1 (**1c**), and among these compounds **2d** and **2e** were the most potent of the series with low nanomolar potencies against the SH-SY5Y neuroblastoma cell line [13]. Several research groups have also reported that the introduction of the small hydrophilic amino group (**2f**) was tolerated at the 5-position of the 3,4-disubstituted pyrazole system [14, 15]. Among the 3,4-diaryl-1-substituted pyrazoles recently synthesized, the 3',4',5'-trimethoxyphenyl)-4-(4'-ethoxyphenyl)-1-methylpyrazole analogue **2g** emerged as a new potent, chemically stable *cis*-restricted derivative of CA-4 [16]. Compound **2g** showed antiproliferative activity of 17 and 31 nM against the human ovarian SKOV and human breast MDA-MD231 cancer cell lines, respectively. This compound was comparable to CA-4 in the tubulin polymerization assay when the two derivatives were tested at the same concentration (10 μM). Harrity et al. have reported two isomer pyrazole-based analogues of CA-4 with the same substitution pattern, corresponding to compounds **2h** and **2i**, with derivative **2h** characterized by a high antiproliferative activity ($IC_{50}$: 5 nM) against human umbilical vein endothelial cells (HUVECs), while isomer **2i** was inactive [17]. Derivatives **2h** and **2i** were also recently synthesized by Zhang et al , who found similar activities for the

two compounds against three human carcinoma cell lines (gastric adenocarcinoma SGC-7901 cells, mouth epidermal carcinoma KB cells and brosarcoma HT-1080 cells), with $IC_{50}$ values ranging from 26 to 60 nM. [18]

In our ongoing efforts to discover new potent antimitotic agents and to extend our knowledge of the pyrazole ring as a suitable mimic for the *cis*-olefin bridge present in CA-4, we report here a pharmacophore exploration and optimization effort around the pyrazole ring. We prepared two different regioisomeric series of 3,4-diarylsubstituted 1*H*-pyrazole derivatives with general structures **3** and **4** (Figure 2). In these two series of designed analogues, obtained by interchanging the substitution pattern of rings A and B, we fixed one of the aryl groups as the 3',4',5'-trimethoxyphenyl motif, identical with the A-ring of CA-4, and the modifications were focused on variation of the substituents at the *para*- position on the second phenyl ring, corresponding to the B-ring of CA-4, with electron-withdrawing ($OCF_3$, $CF_3$) or electron-releasing (Me, Et, n-Pr, MeO, EtO, MeS, EtS) groups (EWG and ERG, respectively). Since the methyl, methoxy and ethoxy groups proved to be favorable for bioactivity, we introduced an additional substituent (F, Cl, Me or MeO) at the *meta*-position of the *para*-methyl/methoxy/ethoxyphenyl ring. Medarde et al have previously reported that the bulky and lipophilic 2-naphthyl moiety can replace the 3'-hydroxy-4'-methoxyphenyl ring B of combretastatin A-4 without significant loss of potency [19]. For this reason, in compound **2c** we evaluated the bioisosteric replacement of the 2'-naphthyl with the 2'-benzo[*b*]thienyl moiety, to obtain derivative **3a**.

The first large series of compounds with general structure **3** was characterized by the presence of a 3',4',5'-trimethoxyphenyl residue at the 3-position of the pyrazole ring combined with a benzo[*b*]thien-2-yl or a phenyl ring with different ERGs or EWGs at the vicinal 4-position of the pyrazole core.

In order to understand whether the substituents at the 3- and 4-positions on the 1*H*-pyrazole nucleus can be interchanged without affecting biological activity, starting from the 4'-tolyl (**3b**), 4'-methoxyphenyl (**3c**) and 4'-ethoxyphenyl (**3p**) derivatives, switching the aryl and 3',4',5'-trimethoxyphenyl moieties, the corresponding regioisomeric derivatives **4a**, **4b** and **4c**, respectively, were synthesized.

A noteworthy point was that the first series of 3-(3',4',5'-trimethoxyphenyl)-4-substituted 1*H*-pyrazoles **3a-r** was concisely synthesized via an efficient and versatile convergent procedure starting from a common key intermediate represented by a 1-tosyl-3-(3',4',5'-trimethoxyphenyl)-4-bromo-1*H*-pyrazole [20].

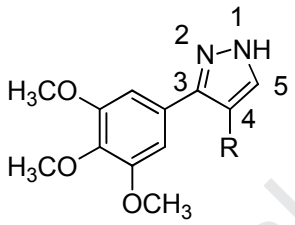


**3a-r**

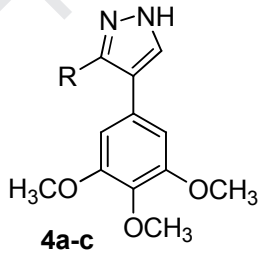


**4a-c**

**3a**, R=benzo[*b*]thien-2'-yl
**3b**, R=4'-$CH_3$-$C_6H_4$
**3c**, R=4'-$CH_3$, 3'-F-$C_6H_4$
**3d**, R=3',4'-$(CH_3)_2$-$C_6H_3$
**3e**, R=4'-$CH_3$, 3'-$OCH_3$-$C_6H_3$
**3f**, R=4'-$CF_3$-$C_6H_4$
**3g**, R=4'-$CH_3CH_2$-$C_6H_4$
**3h**, R=4'-$CH_3(CH_2)_2$-$C_6H_4$
**3i**, R=4'-$OCH_3$-$C_6H_4$
**3j**, R=4'-$SCH_3$-$C_6H_4$
**3k**, R=4'-$OCH_3$, 3'-F-$C_6H_3$
**3l**, R=4'-$OCH_3$, 3'-Cl-$C_6H_3$
**3m**, R=4'-$OCH_3$, 3'-$CH_3$-$C_6H_3$
**3n**, R=4'-$OCH_3$, 3',5'-$(CH_3)_2$-$C_6H_2$
**3o**, R=4'-$OCF_3$-$C_6H_4$
**3p**, R=4'-$OCH_2CH_3$-$C_6H_4$
**3q**, R=4'-$SCH_2CH_3$-$C_6H_4$
**3r,** R=4'-$OCH_2CH_3$, 3'-Cl-$C_6H_3$

**4a**, R=4'-$CH_3$-$C_6H_4$
**4b**, R=4'-$OCH_3$-$C_6H_4$
**4c**, R=4'-$OCH_2CH_3$-$C_6H_4$

**Figure 2.** Structures of 3-(3',4',5'-trimethoxyphenyl)-4-substituted-1*H*-pyrazoles **3a-r** and their isomeric 3-aryl-4-(3',4',5'-trimethoxyphenyl)-1*H*-pyrazole analogues **4a-c**

## 2. Chemistry

3,4-Disubstituted 1*H*-pyrazole derivatives **3a-r** and **4a-c** were synthesized by the general six-step procedure described in Scheme 1. Condensation of 3',4',5'-trimethoxyacetophenone **5** and appropriately substituted acetophenones **6a-c** with dimethylformamide dimethyl acetal (DMF-DMA) provided enaminones **7** and **8a-c**, respectively, in good yields, which were subsequently reacted with hydrazine hydrate in refluxing ethanol to provide the corresponding 3-aryl-1*H*-pyrazole derivatives **9** and **10a-c**. The subsequent regioselective monobromination at the 4-position of the pyrazole nucleus of compounds **9** and **10a-c** with *N*-bromosuccinimide (NBS) in DMF furnished the corresponding 3-aryl-4-bromo-1*H*-pyrazole analogues **11** and **12a-c**, respectively. The pyrazole hydrogen of these latter compounds was temporarily replaced with a tosyl group by treatment with *p*-toluenesulfonyl chloride (TsCl) in a mixture of dichloromethane and pyridine to afford the formation of the key *N*-tosyl-4-bromopyrazole intermediates **13** and **14a-c**, respectively. The brominated products were subjected to a Suzuki cross-coupling process in the presence of the appropriate commercially available arylboronic acid under heterogeneous conditions [$PdCl_2$(DPPF), CsF] in 1,4-dioxane at 65 °C, giving rise to the corresponding 3,4-diaryl pyrazole derivatives **15a-r** and **16a-c**. The tosyl protecting group was then removed by alkaline hydrolysis using a mixture of 1 M aqueous solution of NaOH and ethanol to afford the target 3-(3',4',5'-trimethoxyphenyl)-4-substituted and isomeric 3-aryl-4-(3',4',5'-trimethoxyphenyl)-1*H*-pyrazole derivatives **3a-r** and **4a-c**, respectively.

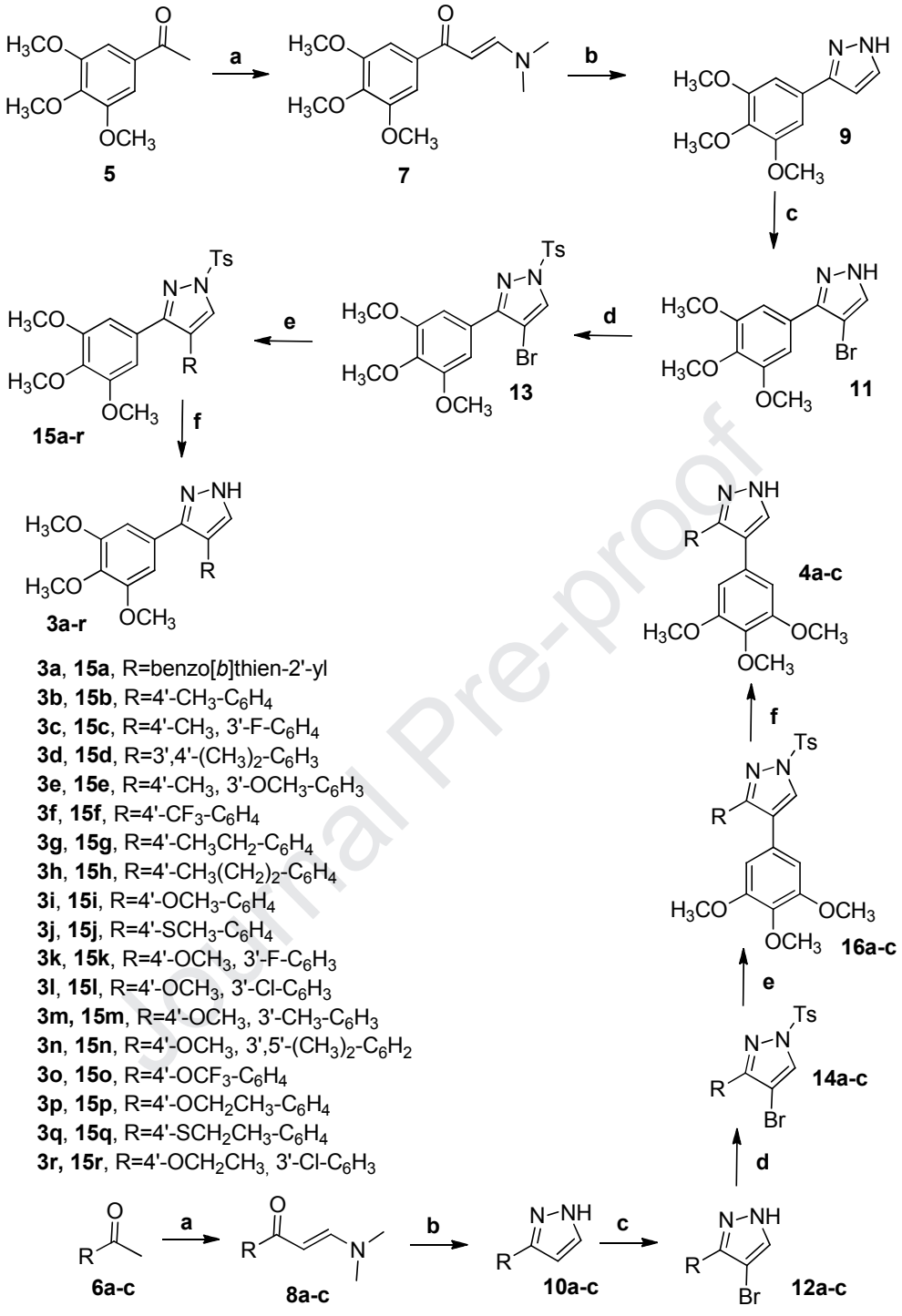


**Scheme 1. Reagents**: **a**: DMF-DMA, DMF, reflux; **b**: $NH_2NH_2{\cdot}H_2O$, EtOH, reflux; **c**: NBS, DMF, room temperature; **d**: TsCl, Py, $CH_2Cl_2$, room temperature, 72 h; **e**: $PdCl_2$(DPPF), $ArB(OH)_2$, CsF, 1,4-dioxane, 65 °C; **f**: 1 M aqueous NaOH, EtOH, 50 °C.

## 3. Biological Results and Discussion

### *3.1. In vitro antiproliferative activities.*

The synthesized 3-(3',4',5'-trimethoxyphenyl)-4-substituted 1*H*-pyrazoles **3a-r** and the corresponding regioisomeric 3-(4'-methyl/methoxy/ethoxyphenyl)-4-(3',4',5'-trimethoxyphenyl)-1*H*-pyrazole analogues **4a**, **4b** and **4c** were evaluated for their ability to inhibit the growth of a panel of six different human cancer cell lines and compared with the previously published 3-(3',4',5'-trimethoxyphenyl)-4-(2'-naphthyl)-1*H*-pyrazole derivative **2c** and the reference compound CA-4 (**1a**) (Table 1).

CA-4 had nanomolar activity against the HeLa, MDA-MB-231, HL-60 and SEM cancer cell lines, while HT-29 and MCF-7 cells were more resistant to CA-4, with $IC_{50}$ values of 3100 and 370 nM, respectively. As shown in Table 1, the antiproliferative activities of most of the tested compounds were less pronounced against MCF-7 cells as compared with the other cell lines. Nevertheless, compounds **3a**, **3i**, **3p**, **3r**, **4b** and, especially, **4c** had excellent activity against MCF-7 cells (the $IC_{50}$ values ranged from 0.2 to17 nM). Excluding compounds **3e**, **3h**, **3n** and **3o**, the tested compounds showed excellent antiproliferative activity against CA-4 resistant HT-29 cells, with $IC_{50}$ values ranging from double-digit to subnanomolar concentrations.

In particular, two of the synthesized compounds, **3p**, bearing a 4'-ethoxyphenyl at the C-4 position of the 1*H*-pyrazole ring, and its isomeric analogue **4c**, exhibited the best antiproliferative activity among the tested derivatives, with $IC_{50}$ values of 0.05-4.5 and 0.06-0.7 nM, respectively, in the six cell lines, as compared with a range of 1-3100 and 3.3-28.4 nM obtained with the reference compounds CA-4 (**1a**) and **2c**. However, compound **4c** was the only compound more active than CA-4 against all cell lines, while the isomeric derivative **3p** was less active than CA-4 against HL-60 cells only. In

addition to highly active compounds **3p** and **4c**, derivatives **3a** and **4b** were more active than CA-4 in five of the six cell lines, again with the exception of the HL-60 cells.

**Table 1.** In vitro inhibitory effects of compounds **2c**, **3a-r**, **4a-c** and CA-4 (**1a**)

| Compound | $IC_{50}$ (nM) | | | | | |
|---|---|---|---|---|---|---|
| | HeLa | HT-29 | MCF-7 | MDA-MB-231 | HL-60 | SEM |
| **3a** | 1.7±0.3 | 7.4±1.9 | 1.4±0.4 | 2.5±0.5 | 2.3±0.3 | 0.5±0.05 |
| **3b** | 11.1±1.7 | 28.2±9.1 | 127.0±34.2 | 10.6±1.6 | 11.9±1.1 | 2.6±0.2 |
| **3c** | 26.2±3.7 | 67.4±14.1 | 1695±450 | 481±26.3 | 31.0±4.5 | 23.5±2.0 |
| **3d** | 35.9±4.5 | 68.4±9.5 | 769±181 | 2606±124 | 51.3±6.2 | 28.5±3.8 |
| **3e** | 286.7±53.2 | 316.1±42.5 | >10000 | 5283±365 | 160.2±22.3 | 305.3±24.8 |
| **3f** | 227.4±45.1 | 67.4±14.1 | 4375±672 | 523±45.6 | 179.0±18.4 | 187.2±26.1 |
| **3g** | 33.5±4.0 | 41.3±7.1 | >10,000 | 3271±326 | 23.3±2.5 | 18.7±1.5 |
| **3h** | 361.3±35.1 | 540.9±55.2 | 2790±535 | 1553±101 | 553±49.1 | 406.1±56.2 |
| **3i** | 6.0±1.2 | 10.5±3.3 | 16.6±4.5 | 8.6±2.1 | 4.4±0.7 | 1.0±0.1 |
| **3j** | 28.7±3.7 | 51.3±8.7 | >10,000 | 3650±254 | 40.9±7.6 | 30.1±3.2 |
| **3k** | 7.3±1.1 | 15.8±2.6 | 805.3±230 | 327±45 | 5.1±0.4 | 2.7±0.25 |
| **3l** | 1.4±0.2 | 0.2±0.05 | 1389±385 | 21.5±1.6 | 17.0±1.9 | 2.4±0.2 |
| **3m** | 32.9±4.0 | 37.3±5.2 | >10000 | 2680±125 | 17.7±1.8 | 17.2±1.4 |
| **3n** | >10,000 | >10,000 | >10,000 | >10,000 | >10,000 | 3340±275 |
| **3o** | 3376±647 | 2416±382 | >10000 | 5740±435 | 1748±270 | 2470±181 |
| **3p** | 0.05±0.0 | 0.3±0.1 | 1.5±0.6 | 4.5±0.9 | 3.2±0.4 | 0.2±0.05 |
| **3q** | 12.5±1.5 | 5.4±1.3 | 492±110 | 31.4±5.6 | 29.7±3.8 | 13.9±1.8 |
| **3r** | 1.6±0.25 | 4.2±0.2 | 4.5±0.08 | 6.9±1.1 | 1.5±0.2 | 1.4±0.2 |
| **4a** | 25.2±3.8 | 44.4±6.3 | 700±165 | 262±15.8 | 31.4±4.2 | 14.7±1.2 |
| **4b** | 1.9±0.3 | 0.8±0.2 | 2.6±0.8 | 0.9±0.2 | 2.1±0.25 | 0.4±0.05 |
| **4c** | 0.07±0.0 | 0.06±0.0 | 0.21±0.07 | 0.7±0.1 | 0.25±0.03 | 0.06±0.0 |
| **2c** | 6.6±1.4 | 8.1±2.3 | 21.4±6.5 | 28.4±1.2 | 9.4±0.9 | 3.3±0.7 |
| **CA-4** (**1a**) | 4.0±1.1 | 3100±100 | 370±100 | 4.5±0.2 | 1.0±0.2 | 5.1±0.1 |

[a]$IC_{50}$= compound concentration required to inhibit tumor cell proliferation by 50%. Values are the mean ± SE from the dose-response curves of at least three independent experiments carried out in triplicate.

In comparing the $IC_{50}$ values, we found that the position of the 3',4',5'-trimethoxyphenyl moiety at either the 3- or 4-position of the 1*H*-pyrazole ring had little effect on antiproliferative activity, since the potency of 3-(3',4',5'-trimethoxyphenyl)-1*H*-pyrazole derivatives **3b**, **3i** and **3p** was comparable and not dramatically reduced as compared with their regioisomers **4a**, **4b** and **4c**, respectively. This is not observed for each couple of regioisomeric heterocyclic mimic cis-stilbene the double bond of CA-4, such as oxazole [21], thiadiazole [22] and imidazole [23]. In examining the effect of switching the position of the two aromatic rings at the 3- and 4-positions on the 1*H*-pyrazole system (**3b** *vs.* **4a**, **3i** *vs.* **4b** and **3p** *vs.* **4c**), with the exception of the two regioisomeric 4'-tolyl derivatives **3b** and **4a** (the latter was from 1.5 to 25-fold less active than the former), the 3-(4'-alkoxyphenyl)-1*H*-pyrazole derivatives **4b** (methoxy) and **4c** (ethoxy) were slightly more active (2-10-fold) than their corresponding 4-(4'-alkoxyphenyl)-1*H*-pyrazole counterparts **3i** and **3p**, respectively, against each cancer cell line. Specifically, for the 4'-ethoxyphenyl isomeric derivatives **3p** and **4c**, this latter compound was from 4- to 6-fold more active than **3p** in five of the six cancer cell lines, the exception being the HeLa cells, in which the two compounds were equipotent. Comparing **3i** and **4b**, which shared a common 4'-methoxyphenyl moiety at the 3- and 4-position of the 1*H*-pyrazole ring, respectively, **4b** was 2- to 13-fold more active than its regioisomeric counterpart **3i.**

Replacement of the 2'-naphthyl by the bioisosteric 2'-benzo[*b*]thienyl ring (compounds **2c** and **3a**, respectively) resulted in a 4- to 15-fold increase in antiproliferative activity against five of the six cell lines, while the difference between these two derivatives was minimal in HT-29 cells. Except in HL-60 cells, **3a** had greater antiproliferative activity

than CA-4, indicating that 2'-benzo[*b*]thienyl moiety, like the 2-naphthyl ring, was a good surrogate for the CA-4 B-ring

The *para*-tolyl derivative **3b** showed interesting antiproliferative activities, with $IC_{50}$ values ranging from 2.6 to 127 nM, with the SEM and MCF-7 cells as the most sensitive and resistant, respectively, to this compound.

Replacement of methyl with the more electron-withdrawing trifluoromethyl moiety (compounds **3b** and **3f**, respectively) resulted in a 2.4-72-fold reduction in antiproliferative activity, which was least pronounced (2-fold) with the HT-29 cells. Encouraged by the activity obtained with compound **3b**, we then synthesized compounds **3c-e** to determine whether various electron-withdrawing or electron-releasing substituents on the phenyl ring would further enhance activity. However, without exception **3c-e** were less active than **3b** in all cell lines.

In an effort to further understand the steric effect of the alkyl substituent at the *para*-position, the ethyl and *n*-propyl derivatives (**3g** and **3h**, respectively) were prepared, resulting in over a 1.5-7-fold loss of activity in four of the six cell lines for the *p*-ethylphenyl homologue **3g** relative to the *p*-tolyl derivative **3b**, with a sharp drop of potency against MCF-7 and MDA-MB-231 cells ($IC_{50}$>10 and 3.3 μM, respectively). The reduction of activity was more pronounced (20-156-fold) against all cell lines by replacing the 4'-methyl group of **3b** with the *n*-propyl group (**3h**), indicating that lengthening the 4'-alkyl chain was not tolerated and caused a significant reduction in antiproliferative activity in all cell lines.

Replacement of the methyl group both of **3b** and its regioisomeric derivative **4a** with a more electron-releasing methoxy moiety (to furnish **3i** and **4b**, respectively) resulted in enhanced antiproliferative activity for **3i**, which was much more pronounced (13-291-

fold) for **4b** against all six cell lines relative to **3b** and **4a**, respectively. For the two derivatives **4a** and **4b**, the greatest differences in activity were 269- and 291-fold in the MCF-7 and MDA-MB-231 cells, respectively.

Replacement of the *para*-methoxy group of **3i** with a weak electron-releasing thiomethyl group, to furnish derivative **3j**, led to a dramatic drop in potency against MCF-7 and MDA-MB-231 cells ($IC_{50}$>10 and 3.6 μM, respectively), while a 5-30-fold reduction in activity was observed against the other four cancer cell lines. A substantial reduction of activity was also observed when the methoxy group was replaced with the strong electron-withdrawing and bulkier trifluoromethoxy moiety (**3o**).

Relative to the activity of **3i**, the insertion of an additional electron-withdrawing (F or Cl) or electron-releasing methyl group at the 3'-position of the 4'-methoxyphenyl ring had varying effects on antiproliferative activity. Introduction of a fluorine atom, to furnish the *p*-OMe, *m*-F derivative **3k**, had little overall effect on antiproliferative activity against HeLa, HL-60 and HT-29 cells, while a 3-, 38- and 50-fold reduction of potency with respect to compound **3i** was observed against SEM, MDA-MB-231 and MCF-7 cells, respectively. The addition of a *meta*-chlorine atom in **3i**, to yield **3l**, had contrasting effects, with a 2-84-fold reduction in activity in four cell lines (most pronounced in MCF-7 cells), while **3l** was 4- and 50-fold more active than **3i** in the HeLa and HT-29 cells, respectively. The cell growth inhibitory activity against four of the six cancer cells was 4-17-fold reduced (and strongly reduced against MCF-7 and MDA-MB-231 cells, with $IC_{50}$>10 and 2.7 μM, respectively) by the introduction of methyl group at the *meta*-position of **3i** (to yield **3m**). Adding a second methyl group, to furnish the *p*-OMe-*m*,*m*'-diMe phenyl derivative **3o**, caused a dramatic decrease in potency relative to **3m** against all cell lines.

Comparing the *para*-alkoxyphenyl derivatives **3i** and **3p** with the corresponding isomeric cognates **4b** and **4c** against each cancer cell line, replacing the methoxy (**3i** and **4b**) with an ethoxy (**3p** and **4c**) moiety resulted in enhanced antiproliferative activities in all cell lines, confirming that the *p*-ethoxyphenyl ring is a good surrogate for the B-ring of CA-4. The enhanced effect on activity resulting from replacement of the methoxy group with an ethoxy moiety in colchicine site was previously observed by us and by others [24].

The *para*-ethoxyphenyl derivative **3p** was 2- to 120-fold more potent than its methoxy counterpart **3i** in five of the six cancer cell lines, while the two compounds had similar activity against HL-60 cells. For the two isomeric derivatives **4b** and **4c**, we found that replacement of methoxy with ethoxy, to furnish derivative **4c**, improved antiproliferative activity 7-27-fold relative to **4b** against five of the six cell lines, with the two compounds being equipotent against MDA-MB-231 cells. Replacement of ethoxy with thioethyl (**3q**) caused a decrease in activity in all cell lines, which was moderate (7-18-fold) against MDA-MB-231, HL-60 and HT-29 cells, and much more pronounced (69-328-fold) against HeLa, MCF-7 and SEM cells.

While the 4'-ethoxy group was favorable for potency, the introduction of an additional *meta*-EWG chlorine group in compound **3p**, resulting in compound **3r**, produced a 1.5-32-fold reduction in antiproliferative activity against five of the six cell lines, the exception being the HL-60 cells, in which **3r** was 2-fold more potent than **3p**. Compound **3r**, as with the corresponding 3-Cl, 4-OMe congener **3l**, was more active than CA-4 in four of the six cell lines, the exceptions being HL-60 and MDA-MB-231 cells.

*3.2. Effects of compounds **3p** and **4c** in nontumor cells.*

To obtain a preliminary indication of the cytotoxic potential of these derivatives in normal human cells, the most active compounds, **3p** and **4c**, were evaluated *in vitro* against peripheral blood lymphocytes (PBL) from healthy donors. Both compounds showed a $GI_{50}$ greater than 10 μM, both in quiescent lymphocytes and in lymphocytes in an active phase of proliferation induced by phytohematoagglutinin (PHA), a mitogenic stimulus (Table 2).

Moreover, since one of the major adverse effects of antimitotics is neurotoxicity, we wanted to evaluate the cytotoxicity of these compounds in normal human astrocytes (NHA). Both compounds again, as shown in Table 2, showed a $GI_{50}$>10 μM, indicating that in this cell line, too, they are not toxic. Altogether, these results suggest that these compounds have very low toxicity in normal cells in comparison to tumor cells, suggesting potential for an excellent therapeutic index.

**Table 2.** Cytotoxicity of compounds **3p** and **4c** for human peripheral blood lymphocytes (PBL) and normal human astrocytes (NHA)

| Compound | $GI_{50}$ (μM)[a] | |
|---|---|---|
| | **3p** | **4c** |
| $PBL_{resting}$[b] | 8.7±0.7 | >10 |
| $PBL_{PHA}$[c] | >10 | >10 |
| NHA | >10 | >10 |

[a] Compound concentration required to inhibit cell growth by 50%.
[b] PBL not stimulated with PHA.
[c] PBL stimulated with PHA.
Values are the mean ± SEM for three separate experiments.

*3.3. Effect of compounds **3p** and **4c** in multidrug-resistant cells.*

To evaluate if compounds **3p** and **4c** are substrates of drug efflux pumps, they were tested against the $CEM^{Vbl-100}$ cell line that is a multidrug-resistant line selected against vinblastine and that overexpress P-glycoprotein (P-gp) [25].

This membrane protein acts as a drug efflux pump and exhibits resistance to a wide variety of structurally unrelated anticancer drugs and other compounds. As shown in Table 3, both compounds showed cytotoxic activity in the $CEM^{Vbl100}$ cells comparable to that of the parental line, indicating that these derivatives are not a substrate for P-gp.

**Table 3.** Cytotoxicity of **3p** and **4c** in multidrug-resistant cells

| Compound | $GI_{50}$ (nM) [a] | |
|---|---|---|
| | $CEM^{wt}$ | $CEM^{Vbl100}$ |
| **3p** | 0.40±0.1 | 1.9±0.2 |
| **4c** | 0.35±0.05 | 0.52±0.1 |

[a] Compound concentration required to reduce cell growth by 50%. Values are the mean ± SEM for three separate experiments.

*3.4. In vitro inhibition of tubulin polymerization and colchicine binding.*

To investigate whether the antiproliferative activities of the most potent compounds of the series derived from an interaction with tubulin, derivatives **3a-d**, **3g**, **3i-m**, **3p-r** and **4a-c** were evaluated for their inhibition of tubulin polymerization and for effects on the binding of [$^3$H]colchicine to tubulin (Table 4). For comparison, CA-4 and **2c** were examined in contemporaneous experiments.

All tested compounds strongly inhibited tubulin assembly, with compound **3a** found to be the most active ($IC_{50}$, 0.30 μM), and it was almost twice as potent as CA-4 ($IC_{50}$, 0.54 μM). Several compounds (**3b**, **3i**, **3p**, **3r**, **4b** and **4c**) were 1.5-fold more potent than CA-4, while all remaining compounds showed activity comparable to that of CA-4.

**Table 4**. Inhibition of tubulin polymerization and colchicine binding by compounds **2c**, **3a-d**, **3g**, **3i-m**, **3p-r**, **4a-c** and CA-4 (**1a**)

| Compound | Tubulin assembly[a] $IC_{50}$±S.D (μM) | Colchicine binding[b] % ±S.D | |
|---|---|---|---|
| | | 5 μM drug | 0.5 μM drug |
| **3°** | 0.30±0.01 | 93±2 | 69±2 |
| **3b** | 0.37±0.04 | 88±0.8 | n.d |
| **3c** | 0.48±0.06 | 91±2 | 49±2 |
| **3d** | 0.61±0.05 | 85±5 | n.d. |
| **3g** | 0.52±0.03 | 85±1 | n.d. |
| **3i** | 0.37±0.06 | 86±0.6 | n.d. |
| **3j** | 0.57±0.02 | 85±4 | n.d. |
| **3k** | 0.42±0.05 | 93±0.8 | 55±2 |
| **3l** | 0.52±0.09 | 85±3 | n.d. |
| **3m** | 0.44±0.09 | 81±0.1 | n.d. |
| **3p** | 0.36±0.01 | 95±0.9 | 69±5 |
| **3q** | 0.48±0.02 | 85±1 | n.d. |
| **3r** | 0.39±0.05 | 90±0.3 | 62±2 |
| **4°** | 0.57±0.01 | 86±5 | n.d. |
| **4b** | 0.34±0.05 | 93±0.8 | 79±2 |
| **4c** | 0.35±0.01 | 96±0.7 | 90±1 |
| **2c** | 0.41±0.04 | 91±4 | 68±0.2 |
| CA-4 (**1a**) | 0.54±0.06 | 97±0.8 | 82±2 |

[a] Inhibition of tubulin polymerisation. Tubulin was at 10 μM.
[b] Inhibition of [$^3$H] colchicine binding. Tubulin and colchicine were at 0.5 and 5 μM concentrations, respectively.
n.d.=not determined

When comparing inhibition of tubulin polymerization with the growth inhibitory effects, we found a good correlation for most, but not all, of the active compounds. While **3b** was generally less potent than **3a** as an antiproliferative agent, the two compounds were similar as inhibitors of tubulin assembly. Although several compounds, such as **3c**, **3d**,

**3g**, **3j**, **3m**, **3r** and **4a** showed lower antiproliferative activity on HeLa, HL-60 and SEM cancer cells when compared with CA-4, they were comparable to CA-4 as inhibitors of tubulin assembly.

In the colchicine binding studies, all compounds when tested at the higher concentration (5 μM) had quantitatively similar effects, varying within a narrow range (81-96% inhibition), and they showed potency comparable to that CA-4, which in these experiments inhibited colchicine binding by 97%. For the most active compounds (90% or higher inhibition when present in the reaction mixture at the same concentration as colchicine), even when tested at a ten-fold reduced concentration (0.5 μM), compounds **4b** and **4c** were as potent as CA-4, which in these latter experiments inhibited colchicine binding by 82%, while derivatives **2c**, **3a**, **3c**, **3k**, **3p** and **3r** were less potent (49-69% range inhibition).

The potent inhibition observed with these compounds indicates that they bind to tubulin at a site overlapping the colchicine site. It is thus significant that one compound (**4c**) in the present series had activities superior to that of CA-4 as inhibitors of tubulin assembly and, less frequently observed, comparable to that CA-4 as inhibitors of colchicine binding to tubulin at the two concentrations (0.5 and 5 μM) tested.

*3.5. Molecular modeling studies.*

Molecular docking studies using Glide SP [26] were conducted on selected compounds to elucidate their potential interaction with the colchicine site of tubulin. The crystal structure of tubulin co-crystallized with the microtubule-destabilizing CA-4 (PDB ID: 5LYJ) was used [27]. The docked molecules occupied the active site similarly to the co-crystallized CA-4, with the trimethoxyphenyl ring deeply buried into the hydrophobic

pocket formed by different residues of the β-tubulin chain, including βVal238, βCys241, βLeu242, βLeu248, βAla250, βLeu255, βAla316, βIle318 and βIle378 (Figure 3). Interestingly, all the new derivatives formed an H-bond between their 4-methoxy group and βCys241, an interaction believed to be fundamental for colchicine site agents. The central pyrazole ring overlapped with the *cis*-double bond of CA-4, confirming its function as a suitable mimic for the *cis*-olefin bridge. The different substituted phenyl rings and the 2'-benzo[*b*]thienyl ring of **3a** were placed in a hydrophobic area formed by the α and β-tubulin interface. Hydrophobic interactions with the surrounding amino acids, including βAsn258, βMet259, βLys352, αThr179, αAla180 and αVal181, further stabilized the molecules in the active site. However, from the docking results, it appeared that this hydrophobic area can accommodate the different substituted phenyl ring, including the *n*-propyl (**3h**) and the tri-substituted (**3n**) derivatives, compounds found not active in the antiproliferative assay. Also, derivatives **3e**, **3f** and **3o** presented a binding mode in line with the other docked molecules, indicating that the loss in antiproliferative activity observed could be associated with some other factors rather than their inability to bind the colchicine site. It should also be noted that the regioisomeric heterocyclic compounds (**3p** *vs*. **4c**) bound in the active site in a similar manner, in line with their ability to inhibit tubulin polymerization.

In order to further elucidate the suggested binding mode and possibly to find a potential structural discriminant between active and inactive compounds, a series of 50 ns molecular dynamic (MD) simulations on selected compounds (**3a, 3e, 3h, 3m, 3n, 3o, 3p, 4c**) were performed using the Desmond software package [28]. The compounds relative binding free energies ($\Delta G_{binding}$) were then calculated using the Prime/MM-GBSA based calculation method [29, 30]. All the protein-ligand systems reached

stability after an initial 25 ns of equilibration, as shown by the C-alpha RMSD variation, and therefore only the second 25 ns of the simulation was considered in our analysis. In general, the position of the trimethoxyphenyl ring and the interaction between the 4-methoxy group and βCys241 were maintained by all the derivatives during the entire MD, potentially contributing to the protein-ligand stability. The orientation of the different substituted phenyl rings and 2'-benzo[*b*]thienyl group (**3a)** in the nearby hydrophobic area was constant during the entire simulation, with the hydrophobic interactions with the surrounding residues maintained. Unfortunately, the $\Delta G_{binding}$ calculated values for all the ligand-protein complexes were very similar and not significantly different to justify a potential correlation between the biological activity and the calculated values. In conclusion, molecular docking and MD studies have given insight into the potential binding mode for this family of compounds, but both molecular modeling techniques were not able to find a significant correlation between the calculated binding energy values and the experimental antiproliferative data. Other factors, such as physical-chemical properties of the compounds rather than their ability to interact with tubulin could be the cause of the loss of biological activity seen in the cell-based assays.

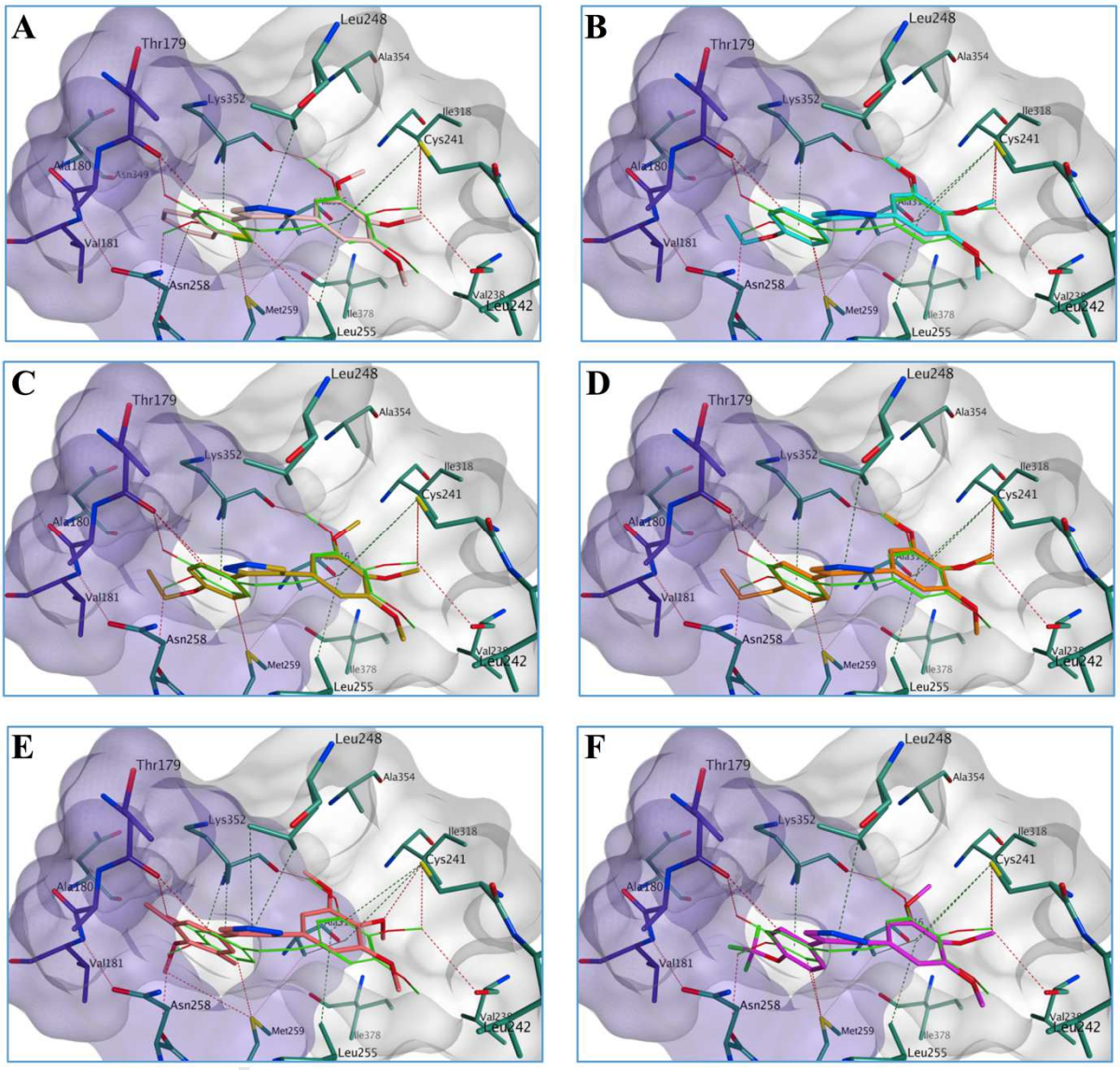


**Figure 3.** Proposed binding modes for compounds **3a** (**A**), **3p** (**B**), **4c** (**C**), **3h** (**D**), **3n** (**E**), **3o** (**F**) in comparison with CA-4 in the tubulin colchicine site (PDB ID: 5LYJ). Co-crystallized CA-4 is shown in green, compound **3a** in pink, compound **3p** in turquoise, compound **4c** in gold, compound **3h** in orange, compound **3n** in salmon and compound **3o** in purple. The carbon atoms of residues from α-tubulin chain are shown in dark purple, whereas carbon atoms of residues from β-tubulin are colored in green. The hydrophobic area at the dimer interface is represented as a light purple surface.

*3.6. Compounds **3p** and **4c** induced cell cycle arrest in G2/M along with alteration of cell cycle checkpoint proteins.*

The effects of two of the most active compounds (**3p** and **4c**) on cell cycle progression was examined by flow cytometry in MDA-MB-231 cells (Figure 4). After a 24 h

treatment, both compounds induced a G2/M arrest in these cells, but **4c** (Figure 4, Panel B) was more potent than **3p** since a maximum effect (60% G2/M cells) occurred with 10 nM **4c**. A comparable effect with **3p** required 100 nM compound. With both compounds, the increase in G2/M cells was accompanied by an equivalent reduction of cells in the S and G1 phases.

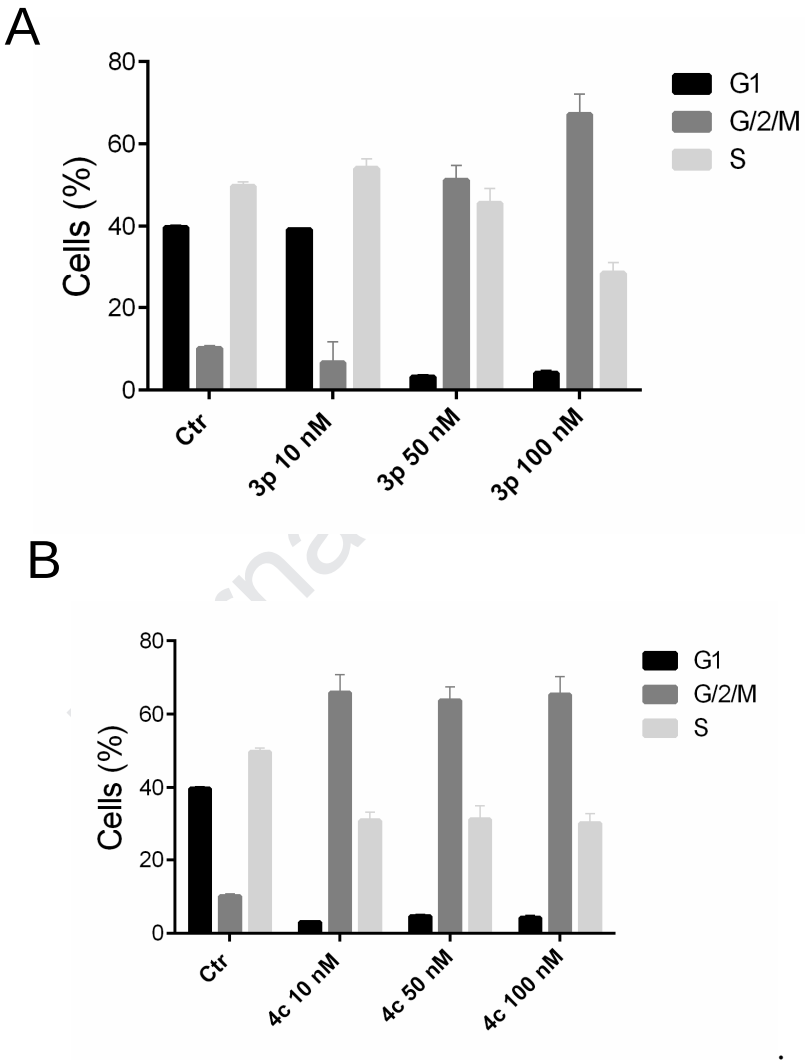


**Figure 4.** Cell cycle analysis of MDA-MB-231 cells treated with **3p** (Panel A) or **4c** (Panel B) for 24 h, at the indicated concentrations. Cells were fixed and labeled with PI and analyzed by flow cytometry as described in the Experimental Section. Data are represented as mean of two independent experiments ± SEM.

To further investigate the effects of the two compounds on the cell cycle, we evaluated the expression of proteins involved in regulation of the cell cycle and in spindle

assembly in MDA-MB-231 cells by western blot analysis. As shown in Figure 5, both compounds induced a substantial increase in the expression of p21, a well known cyclin dependent kinase inhibitor. Although it is known that a p21 increase contributes to arrest cells in G1, a p21 increase can also inhibit cdc2-cyclin B complex formation and thus contribute to mitotic arrest [31].

Moreover, cdc25c expression was strongly reduced, in particular with **4c** (Figure 5 Panel B) both after 24 and 48 h treatments even at the lower concentration (50 nM) used. Similarly, there was also a decrease in the dephosphorylation of cdc2. Note that dephosphorylation of this protein is needed to activate the cdc2/cyclin B complex, and this effect is stimulated by cdc25c [32, 33]. On the other hand, neither compound caused a significant change in cyclin B expression after either a 24 or 48 h treatment. This suggests that the induced G2/M arrest is not due to defects in G2/M regulatory proteins but, rather, is closely linked with acceleration of entry into mitosis. These results are in agreement with findings with other antimitotic derivatives synthesized by our group [34-36] and suggest that cdc2/cyclin B1 complexes failed to be activated, preventing cells from exiting mitosis, which would eventually lead to apoptotic cell death.

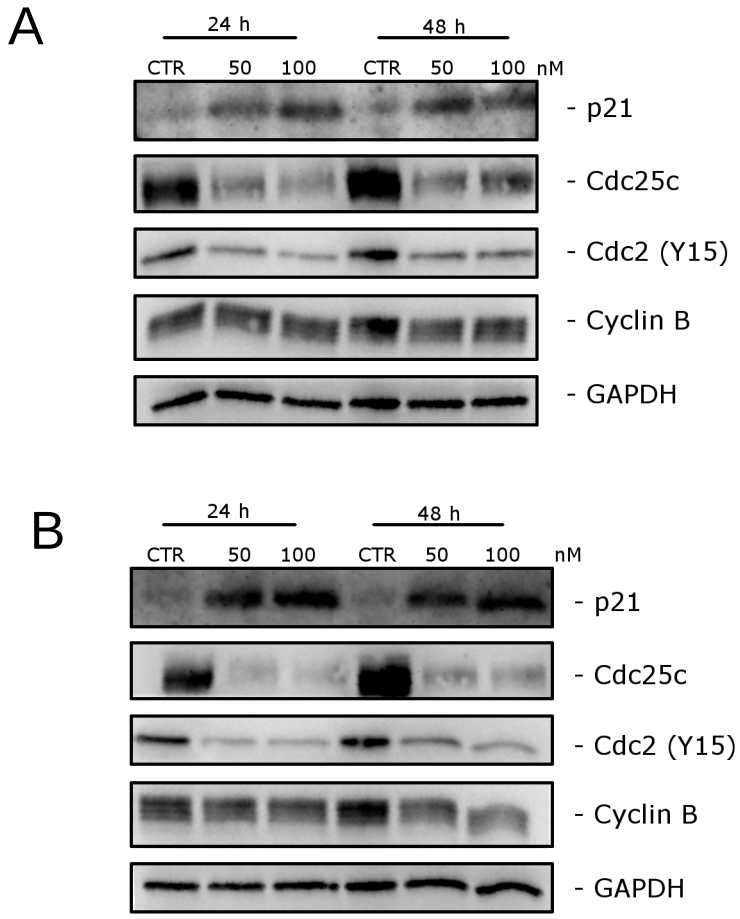


**Figure 5.** Effect of compounds **3p** (Panel A**)** and **4c** (Panel B) on cell cycle checkpoint proteins. MDA-MB-231 cells were treated for 24 or 48 h with the indicated concentrations of compounds. The cells were harvested and lysed for detection of the expression of the indicated protein by western blot analysis. To confirm equal protein loading, each membrane was stripped and reprobed with anti-GAPDH antibody.

*3.7. Compounds **3p** and **4c** induced apoptosis.*

To evaluate the mode of cell death induced by **3p** and **4c**, we performed a bi-parametric cytofluorimetric analysis using propidium iodide (PI) and annexin-V-FITC, which stain DNA and phosphatidylserine (PS) residues, respectively. We analysed the effects on apoptosis induction by both these molecules in MDA-MB-231 cells after treatments for 24 or 48 h.

Both compounds induced apoptosis in a time and concentration dependent manner (Figure 6). The apoptotic effects were evident with both compounds at the lowest concentration examined (50 nM).

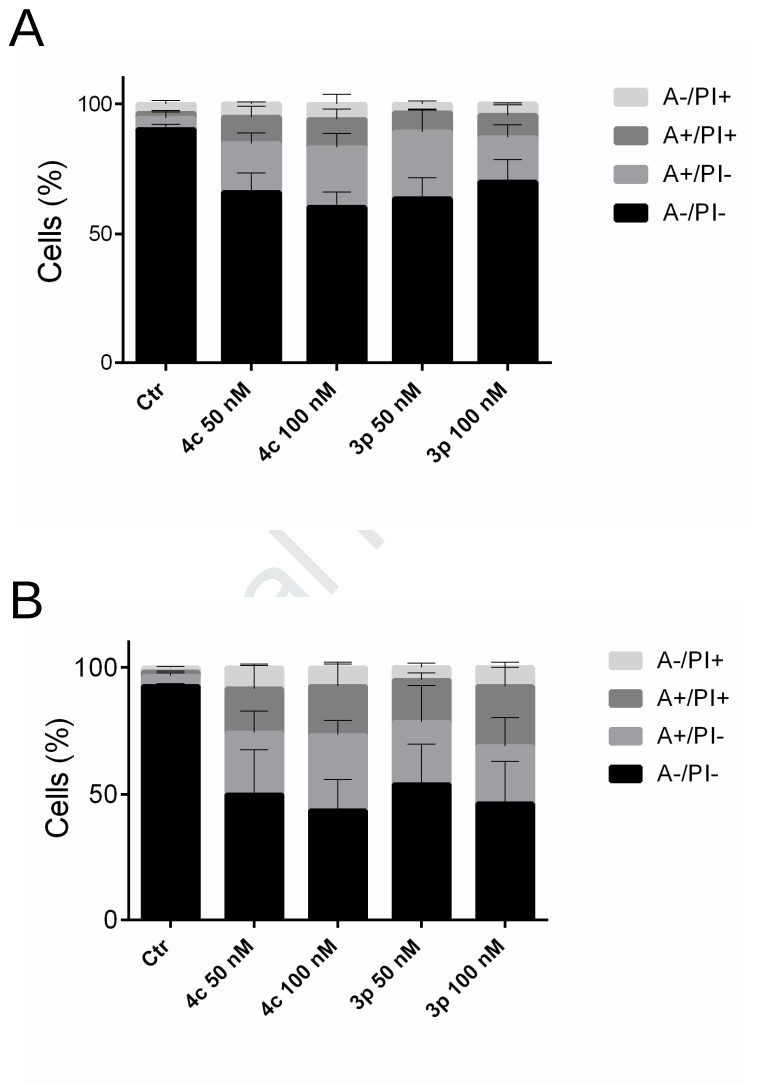


**Figure 6.** Flow cytometric analysis of apoptotic cells after treatment of MDA-MB-231 cells with compounds **4c or 3p** at the indicated concentrations after incubation for 24 (Panel A) or 48 h (Panel B). The cells were harvested and labeled with annexin-V-FITC and PI and analyzed by flow cytometry. Dual staining for annexin-V and with PI permits discrimination between live cells (annexin-$V^-/PI^-$), early apoptotic cells (annexin-$V^+/PI^-$), late apoptotic cells (annexin-$V^+/PI^+$) and necrotic cells (annexin-$V^-/PI^+$). Data are represented as mean ± SEM of three independent experiments.

*3.8. Apoptosis induced by compounds **4c** and **3p** follows the mitochondrial pathway.*

Since many antimitotic derivatives induce apoptosis through the mitochondrial pathway [37], we investigated if **4c** and **3p** also induced mitochondrial depolarization. We treated MDA-MB-231 cells with **4c** or **3p** at 50 or 100 nM for 24 or 48 h. The mitochondrial potential was evaluated by flow cytometry using the fluorescent dye JC-1 [38]. As shown in Figure 7 (Panel A), at 24 h there was only a small increase in mitochondrial depolarization, represented as percentage of monomeric JC-1, whereas at 48 h the increase became significant, in agreement with the annexin-V apoptotic assay. Since the mitochondrial depolarization is associated with production of reactive oxygen species (ROS) [39-41], we also evaluated whether ROS production increased after treatment with either compound. We analyzed cellular ROS levels using the dye 2,7-dichlorodihydrofluorescein diacetate ($H_2$-DCFDA), which is oxidized to the fluorescent compound dichlorofluorescein (DCF) upon ROS induction.

The results shown in Figure 7 (Panels A and B) indicated that both compounds significantly increased ROS production in comparison with the amounts observed in control MDA-MB-231 cells, in good agreement with the mitochondrial depolarization described above.

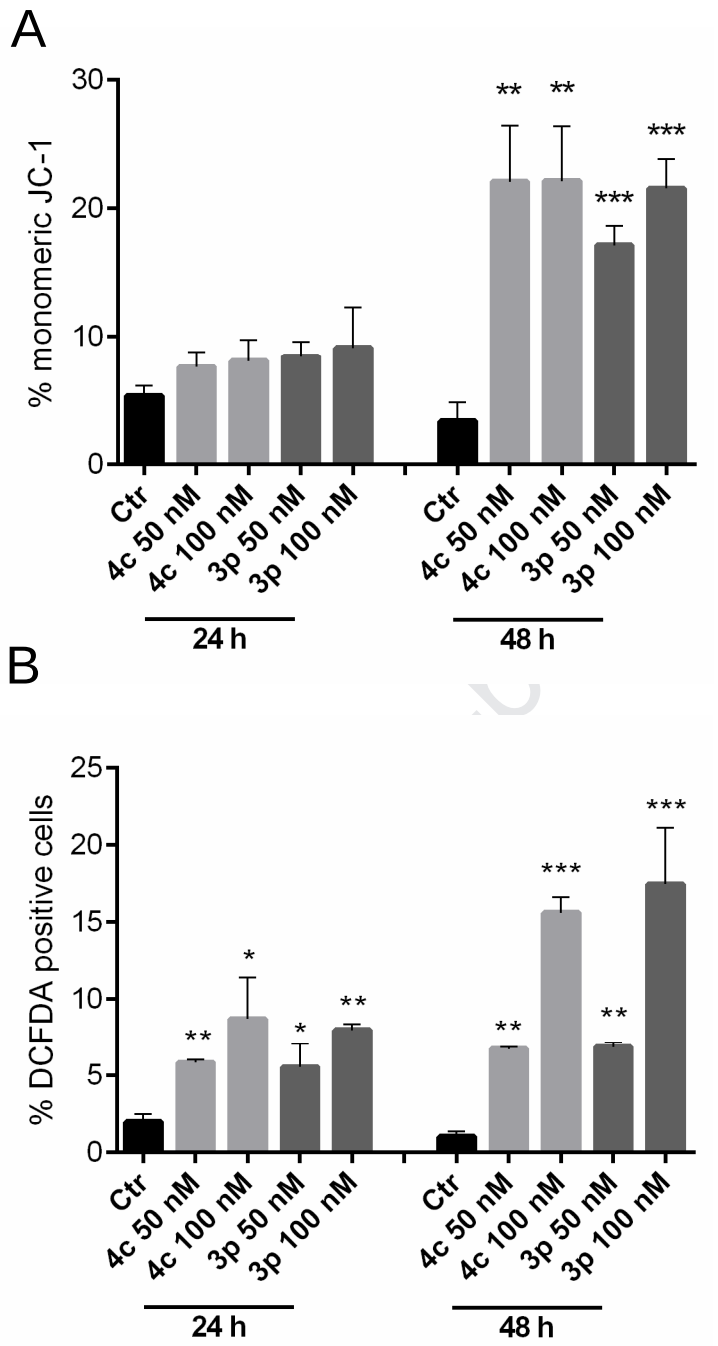


**Figure 7.** Panel A. Analysis of mitochondrial membrane potential ($\Delta\psi_{mt}$) after treatment of MDA-MB-231 cells with **3p** or **4c**. Cells were treated with the indicated concentrations of **3p** and **4c** for 24 or 48 h and then stained with the fluorescent probe JC-1. Cells were then analyzed by flow cytometry as described in the experimental section. Data are presented as mean ± SEM of three independent experiments. Panel B. Analysis of ROS production after treatment of HeLa cells with **3p** or **4c**. Cells were treated with the indicated concentrations of **3p** or **4c** for 24 or 48 h and then stained with $H_2$-DCFDA. Cells were then analyzed by flow cytometry as described in the experimental section. Data are represented as mean ± SEM of three independent experiments. *p<0.05; **p<0.01; ***p<0.001 vs respective control.

*3.9. Compounds **3p** and **4c** induce PARP cleavage and down regulation of Xiap and MCL-1*

To further study the apoptotic process induced by the two compounds, we evaluated the activation of poly ADP-ribose polymerase (PARP). As shown in Figure 8, both compounds in MDA-MB-231 cells caused a significant cleavage of PARP after a 48 h treatment, confirming their pro-apoptotic activity.

We also investigated the expression of anti-apoptotic proteins, such as Mcl-1 and X-linked inhibitor of apoptosis protein (Xiap). Mcl-1 is an anti-apoptotic member of the Bcl-2 family, levels of which regulate sensitivity to antimitotic drugs [42]. As shown in Figure 8 (Panel A) we observed only a slight reduction of Mcl-1 expression with **3p** at the later incubation time (48 h). In contrast, strong reduction was observed for **4c** after a 24 h treatment and at the lower concentration used (50 nM).

Xiap is a member of the IAP family (inhibitors of apoptosis protein). Generally, the IAPs function through direct interactions to inhibit the activity of several caspases, thereby inhibit the processing and activation of these enzymes and leading to inhibition of apoptosis [43].

Our findings (Figure 8, Panels A and B) showed that expression of Xiap almost disappeared with both compounds even at the lower concentration examined. Altogether, these results suggest that these compounds result in the downregulation of both Mcl-1 and Xiap to disable their anti-apoptotic functions.

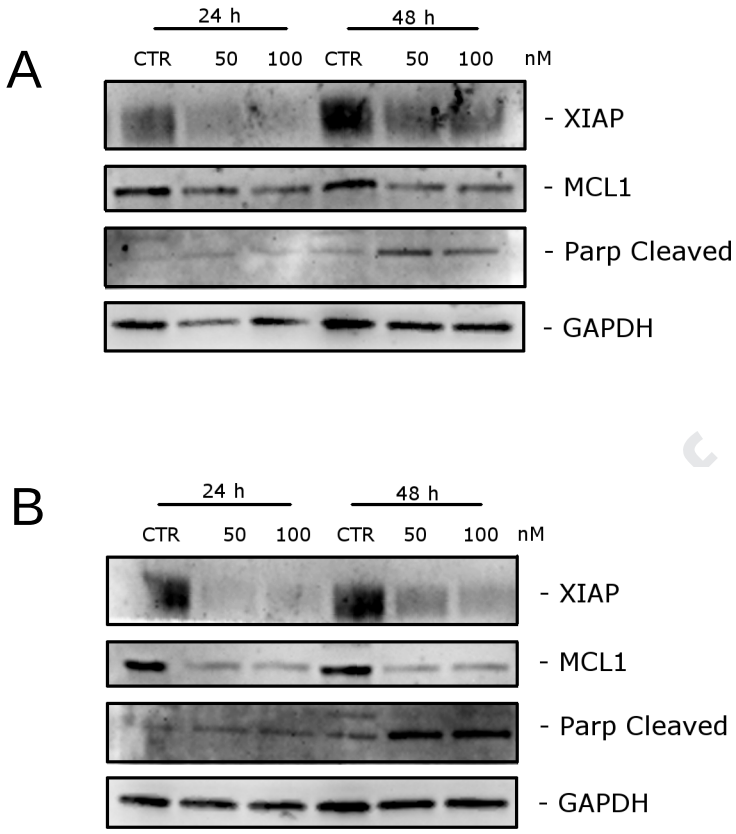


**Figure 8.** Compounds **3p** (Panel A) and **4c** (Panel B), induce PARP cleavage and down regulation of the anti-apoptotic proteins XIAP and MCL-1. MDA-MB-231 cells were treated for 24 or 48 h with the indicated concentrations of compounds. The cells were harvested and lysed for detection of the expression of the indicated protein by western blot analysis. To confirm equal protein loading, each membrane was stripped and reprobed with anti-GAPDH antibody.

*3.10. Compounds **3p** and **4c** impair cell migration in MDA-MB-231 cells.*

We evaluated **3p** and **4c** for their ability to reduce cell migration of MDA-MB-231 cells, which are highly metastatic. Tumor cell migration is an important step in the metastatic process, and microtubules play a fundamental role in cell motility. Figure 9A shows representative images of the wound-healing assay in MDA-MB-231 cells treated with 20 nM **3p** or 5 nM **4c**. Monitoring cell movement at 24 and 48 h, we observed a strong reduction of cell migration, particularly with compound **4c**. Note that inhibition of the

migratory process was obtained at concentrations that *per se* do not induce apoptosis, suggesting a potent inhibitory effect of **4c** on microtubule dynamics.

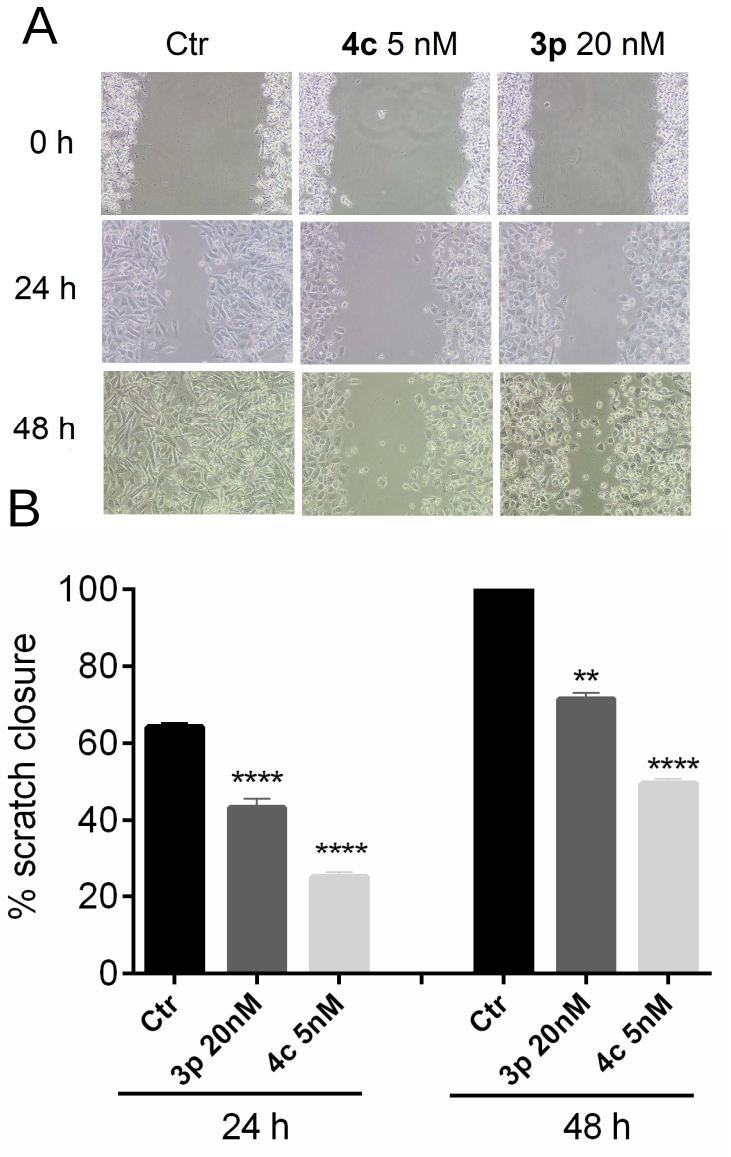


**Figure 9.** Panel A. Confluent MDA-MB-231 cell monolayer was scratched and treated with **4c** or **3p** at 5 or 20 nM, respectively, and monitored for 24 and 48 h, Representative images of wound closure at 24 and 48 h. 10× magnification. Panel B. Relative quantification of the distance between scratch edges. Data are represented as mean ± SEM of four independent experiments. **p<0.01; ****p<0.0001 vs respective control.

*3.11. Compound **4c** reduced tumor growth in a mouse allograft tumor model.*

The antitumor effect *in vivo* of compound **4c** was evaluated in an allograft tumor model developed in mice [44]. This model consists of the use of EO771 murine breast cancer cells that are injected orthotopically into the mammary fat pad of C57BL/6 female mice. Compound **4c** was administered by the intraperitoneal route every other day at two different doses (5.0 and 15 mg/kg). As reference compound, CA-4P (**1b**) was used at the dose of 30 mg/kg. The results shown in Figure 10 indicated that the compound is able to significantly reduce tumor burden in a dose-dependent manner, even at the lower dose tested (5.0 mg/kg). In particular, a highly significant reduction of tumor mass was observed not only versus the control but also towards CA-4P ($p<0.01$). Moreover, even at the higher dose (15 mg/kg), **4c** did not show any sign of toxicity and did not cause a decrease in animal body weight (Figure 10, Panel C).

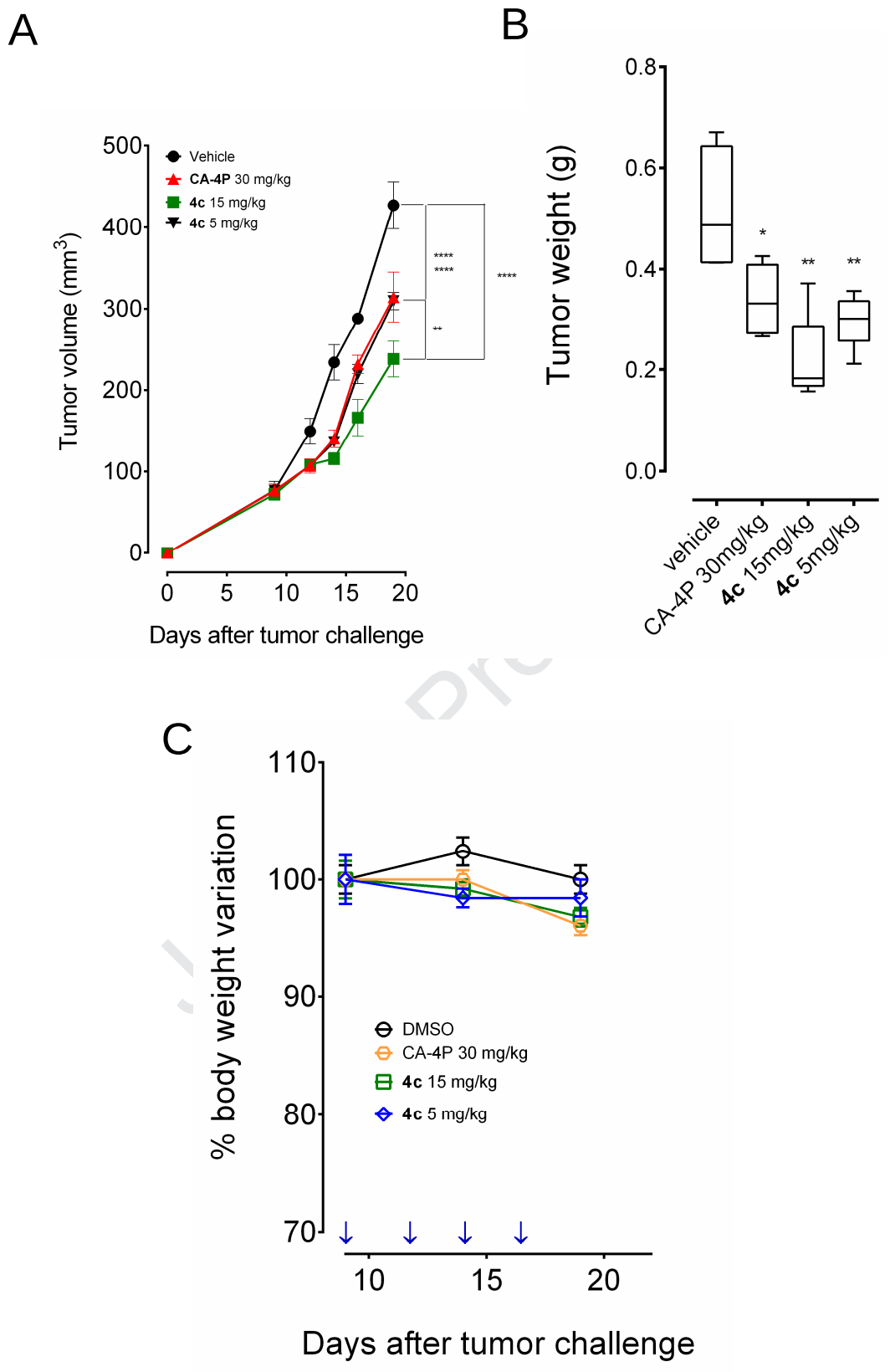


**Figure 10.** Inhibition of mammary tumor growth by compound **4c** in a syngeneic orthotopic E0771-C57BL/6 mouse model. Female C57BL/6 mice were injected orthotopically with $10^6$ EO711 murine breast cancer cells.

Tumor-bearing mice were administered the vehicle, as control, or 15 and 5.0 mg/kg of **4c** and CA-4P as reference compound at the dose of 30 mg/kg. Injections were given intraperitoneally on the days indicated by the arrows. Data are presented as mean ± SEM of tumor volume at each time point for 5 animals per group. Asterisks indicate a significant difference between the treated and the control group. * $p < 0.05$, ** $p < 0.001$, **** $p < 0.0001$. A. Tumor volume. B. Tumor weight. C. Body weight as a measure of toxicity.

## 4. Conclusions

We focused our work here on the preparation of two series of 3,4-diaryl pyrazole derivatives characterized by the presence of a common 3',4',5'-trimethoxyphenyl ring at either the C-3 or C-4 position of the 1*H*-pyrazole ring. We proposed that the 3,4-diarylsubstituted 1*H*-pyrazole ring could serve as a suitable mimic to retain the bioactive configuration afforded by the *cis*-double bond present in CA-4. For both these series of compounds, the 3',4',5'-trimethoxyphenyl and 1*H*-pyrazole rings mimic the ring A and *cis*-double bond of CA-4, respectively, while a 2'-benzo[*b*]thienyl or phenyl ring substituted with electron-releasing or electron-withdrawing groups was utilized as a B-ring surrogate to mimic the 3'-hydroxy-4'-methoxyphenyl group in CA-4. The flexible synthetic method that we developed permitted the generation of a large family of 4-substituted-3-(3',4',5'-trimethoxyphenyl)-1*H*-pyrazole derivatives starting from a common 1-tosyl-3-(3',4',5'-trimethoxyphenyl)-4-bromo-1*H*-pyrazole intermediate. In the second series of compounds, starting from derivatives **3b**, **3i** and **3p**, we switched two aromatic rings at the 3- and 4-positions of the 1*H*-pyrazole ring and synthesized the corresponding isomers **4a**, **4b** and **4c**, respectively.

It is clear that the substitution pattern on the phenyl either at the 3- or 4-position of the 1*H*-pyrazole ring plays an important role for antitubulin and antiproliferative activities, and this was supported by the molecular docking studies. The activity of most of the synthesized compounds was not affected by the relative resistance of HT-29 and MCF-7

cells to CA-4. Generally, either two (**3c-e**, **3k-m** and **3q**) or three substituents (**3n**) on the phenyl group led to a reduction in antiproliferative activity, suggesting that steric factors account for the loss of activity observed with these compounds. The results demonstrated that the 4'-ethoxy substituent on the second phenyl ring either at the 3- or the 4-position of the 1*H*-pyrazole nucleus (compounds **3p** and **4c**) could replace the B-ring of CA-4. Derivatives **3p** and **4c** had the best antiproliferative activities against the cell lines we examined and, overall, were more active than CA-4, with the exception of derivative **3p**, which was 3-fold less active than CA-4 but only against HL-60 cells. In particular, the 3-(4'-ethoxyphenyl)-4-(3',4',5'-trimethoxyphenyl)-1*H*- derivative **4c** exhibited $IC_{50}$ values ranging from 0.05 to 0.7 nM against the cell lines examined, as compared with the range of 1-3100 nM obtained with CA-4. Compound **4c** was one the most potent inhibitors of tubulin polymerization and an exceptionally potent inhibitor of colchicine binding ($IC_{50}$=0.35 μM for assembly, 96 and 90% inhibition of the binding of [$^3$H]colchicine at the concentrations of 5 and 0.5 μM, respectively).

These studies identified tubulin as the molecular target of these compounds, since those with the greatest inhibitory effects on cell growth strongly inhibited tubulin assembly and the binding of colchicine to tubulin. In the series of tested compounds (**3a-d**, **3g**, **3i-m**, **3p-r** and **4a-c)**, inhibition of [$^3$H]colchicine binding correlated more closely with inhibition of tubulin assembly than with antiproliferative activity.

Comparing pairs of regioisomeric derivatives (**3b** *vs.* **4a**, **3i** *vs.* **4b** and **3p** *vs.* **4c**), it is evident that the presence of the 3',4',5'-trimethoxyphenyl moiety at the 3- or 4-position of the pyrazole ring seemed not critical for antiproliferative as well as for tubulin polymerization inhibitory activity, with the two isomeric compounds **3p** and **4c**

exhibiting potent tubulin polymerization inhibitory activity as well as antiproliferative activity superior to that of CA-4.

## 5. Experimental Protocols.

### *5.1. Chemistry.*

#### *5.1.1. Materials and Methods.*

$^{1}H$ experiments were recorded on either a Bruker AC 200 or a Bruker Avance III 400 spectrometer, while $^{13}C$ NMR spectra were recorded on a Varian 400 Mercury Plus or a Bruker Avance III 400 spectrometer. Chemical shifts (δ) are given in ppm upfield, and the spectra were recorded in appropriate deuterated solvents, as indicated. Mass spectra were recorded by an ESI single quadrupole mass spectrometer Waters ZQ 2000 (Waters Instruments, UK), and the values are expressed as $[M+1]^{+}$. Melting points (mp) were determined on a Buchi-Tottoli apparatus and are uncorrected. All products reported showed $^{1}H$ and $^{13}C$ NMR spectra in agreement with the assigned structures. The purity of tested compounds was determined by combustion elemental analyses conducted by the Microanalytical Laboratory of the Chemistry Department of the University of Ferrara with a Yanagimoto MT-5 CHN recorder elemental analyzer. All tested compounds yielded data consistent with a purity of at least 95% as compared with the theoretical values. Reaction courses and product mixtures were routinely monitored by TLC on silica gel (precoated $F_{254}$ Merck plates), and compounds were visualized with aqueous $KMnO_4$. Flash chromatography was performed using 230-400 mesh silica gel and the indicated solvent system. Organic solutions were dried over anhydrous $Na_2SO_4$.

#### *5.1.2. General method A for the synthesis of compounds **7** and **8a-c**.*

A mixture of the appropriate acetophenone **5** or **6a-c** (5 mmol) and DMF-DMA (2.7 mL, 2.38 g., 20 mmol, 4 equiv.) in DMF (2 mL) was stirred at 150 °C for 24 h. The reaction mixture was evaporated *in vacuo*, the crude residue suspended with diethyl ether and the suspension stirred for 15 min. The solid was filtered and used without further purification for the next reaction. Compounds **7** and **8a-b** showed spectroscopic and analytical data in agreement with those previously published [45].

*5.1.2.1. (E)-3-Dimethylamino-1-(4-ethoxyphenyl)-prop-2-en-1-one (**8c**).* Synthesized according to procedure A, compound **8c** was isolated as a yellow solid. Yield 68%, mp 110-112 °C. $^{1}$H-NMR ($CDCl_3$) δ: 1.43 (t, J=7.0 Hz, 3H), 3.06 (s, 3H), 3.15 (s, 3H), 4.06 (q, J=7.0 Hz, 2H), 5.70 (d, J=12.2 Hz, 1H), 6.87 (d, J=7.0 Hz, 2H), 7.87 (d, J=7.0 Hz, 2H), 8.02 (d, J=12.2 Hz, 1H). MS (ESI): $[M+1]^+$=220.3.

*5.1.3. General method B for the preparation of compounds **9** and **10a-c**.*

A mixture of the appropriate (*E*)-3-dimethylamino-1-aryl-prop-2-en-1-one **7** or **8a-c** (3 mmol) and hydrazine hydrate (0.18 mL, 0.18 g, 3.6 mmol, 1.2 equiv.) in ethanol (15 mL) was stirred at reflux for 4 h. The solvent was removed, the residue dissolved with dichloromethane (15 mL), and the solution washed sequentially with water (10 mL) and brine (10 mL). The organic layer was dried, filtered and concentrated under reduced pressure, and the residue was purified by flash column chromatography on silica gel. For the characterization of compounds **9** and **10a-b** see reference [46].

*5.1.3.1. 3-(4-Ethoxyphenyl)-1H-pyrazole (**10c**).* Synthesized according to procedure B, the crude residue was purified by flash chromatography, using ethyl acetate:petroleum ether 6:4 (v:v) as eluent, to furnish **10c** as a white solid. Yield: 95%, mp 90-92 °C. $^{1}$H-NMR ($CDCl_3$) δ: 1.43 (t, J=7.0 Hz, 3H), 4.08 (q, J=7.0 Hz, 2H), 6.54 (d, J=2.2 Hz, 1H),

6.92 (d, J=8.6 Hz, 2H), 7.62 (d, J=2.2 Hz, 1H), 7.69 (d, J=8.6 Hz, 2H), 9.17 (bs, 1H). MS (ESI): $[M]^+$=189.0.

*5.1.4. General method C for the synthesis of compounds **11** and **12a-c**.*

A solution of the appropriate 3-aryl-1*H*-pyrazole **9** or **10a-c** (1 mmol) in DMF (2 mL) was treated with NBS (0.18 g, 1 mmol) in small portions. After 90 min at room temperature, the reaction mixture was evaporated under reduced pressure and the resulting residue dissolved with $CH_2Cl_2$ (10 mL), which was washed with a saturated solution of $NaHCO_3$ (5 mL) and brine (5 mL), dried and evaporated. The residue was purified by column chromatography on silica gel.

*5.1.4.1. 4-Bromo-3-(3,4,5-trimethoxyphenyl)-1H-pyrazole (**11**).* Synthesized according to procedure C, the crude residue purified by flash chromatography, using EtOAc:petroleum ether 8:2 (v:v) for elution, furnished **11** as a white solid. Yield 82%, mp 174-175 °C $^1$H-NMR (DMSO-$d_6$) δ: 3.70 (s, 3H), 3.83 (s, 6H), 7.09 (s, 2H), 8.08 (s, 1H), 13.3 (bs, 1H). MS (ESI): $[M]^+$=313.1, $[M+2]^+$=315.2.

*5.1.4.2. 4-Bromo-3(5)-(p-tolyl)-1H-pyrazole (**12a**).* Synthesized according to procedure C, the crude residue purified by flash chromatography, using EtOAc:petroleum ether 3:7 (v:v) for elution, furnished **12a** as a white solid. Yield 72%, mp 110-112 °C. $^1$H-NMR ($CDCl_3$) δ: 2.17 (s, 3H), 7.34 (d, J=8.2 Hz, 2H). 7.83 (d, J=8.2 Hz, 2H), 8.31 (s, 1H), 12.0 (bs, 1H). MS (ESI): $[M]^+$=237.1, $[M+2]^+$=239.1.

*5.1.4.3. 4-Bromo-3(5)-(4-methoxyphenyl)-1H-pyrazole (**12b**).* Synthesized according to procedure C, the crude residue purified by flash chromatography, using EtOAc:petroleum ether 1:1 (v:v) for elution, furnished **12b** as a white solid. Yield 90%,

mp 78-80 °C. $^1$H-NMR (DMSO-$d_6$) δ: 3.80 (s, 3H), 7.02 (d, J=6.8 Hz, 2H), 7.69 (d, J=6.8 Hz, 2H), 7,84 (bs, 1H), 13.4 (bs, 1H). MS (ESI): $[M]^+$=253.1, $[M+2]^+$=255.1.

*5.1.4.4. 4-Bromo-3-(4-ethoxyphenyl)-1H-pyrazole (**12c**).* Synthesized according to C, the crude residue purified by flash chromatography, using EtOAc:petroleum ether 1:1 (v:v) for elution, furnished **12c** as a white solid. Yield 86%, mp 96-97 °C. $^1$H-NMR (DMSO-$d_6$) δ: 1.31 (t, J=7.0 Hz, 3H), 4.04 (q, J=7.0 Hz, 2H), 6.97 (d, J=8.4 Hz, 2H), 7.63 (d, J=8.4 Hz, 2H), 8.04 (s, 1H), 13.3 (bs, 1H). MS (ESI): $[M]^+$=266.9, $[M+2]^+$=269.0.

*5.1.5. General method D for the synthesis of compounds **13** and **14a-c**.* A solution of the appropriate 4-bromo-3-aryl-1*H*-pyrazole **11** or **12a-c** (2.1 mmol) and pyridine (0.51 mL, 6.3 mmol, 3 equiv.) in dichloromethane (5 mL) was treated with TsCl (0.48 g, 2.52 mmol, 1.2 equiv.) in one portion and then stirred at room temperature for 72 h. The mixture was diluted with $CH_2Cl_2$ (10 mL), washed with a 0.1 N aqueous solution of HCl (5 mL), then a saturated solution of $NaHCO_3$ (5 mL) and brine (5 mL), dried and evaporated under reduced pressure. The residue was purified by column chromatography on silica gel.

*5.1.5.1. 4-Bromo-1-tosyl-3-(3,4,5-trimethoxyphenyl)-1H-pyrazole (**13**).* Following general procedure D, the crude residue purified by flash chromatography, using EtOAc:petroleum ether 2:8 (v:v) for elution, furnished **13** as a white solid. Yield 89%, mp 121-123 °C. $^1$H-NMR ($CDCl_3$) δ: 2.42 (s, 3H), 3.87 (s, 3H), 3.89 (s, 6H), 7.08 (s, 2H), 7.32 (d, J=8.2 Hz, 2H), 7.91 (d, J=8.2 Hz, 2H), 8.18 (s, 1H). MS (ESI): $[M]^+$=467.0, $[M+2]^+$=468.8.

*5.1.5.2. 4-Bromo-3-(p-tolyl)-1-tosyl-1H-pyrazole (**14a**).* Following general procedure D, the crude residue purified by flash chromatography, using EtOAc:petroleum ether 3:7 (v:v) for elution, furnished **14a** as a white solid. Yield 89%, mp 90-92 °C. $^1$H-NMR ($CDCl_3$) δ: 2.34 (s, 3H), 2,44 (s, 3H), 6.82 (d, J=9.0 Hz, 2H), 7.24 (d, J=8.4 Hz, 2H), 7.64 (d, J=9.0 Hz, 2H), 7.80 (d, J=8.4 Hz, 2H), 8.00 (s, 1H). MS (ESI): $[M]^+$=391.3, $[M+2]^+$=393.3.

*5.1.5.3. 4-Bromo-3-(4-methoxyphenyl)-1-tosyl-1H-pyrazole (**14b**).* Following general procedure D, the crude residue purified by flash chromatography, using EtOAc:petroleum ether 4:6 (v:v) for elution, furnished **14b** as a white solid. Yield >95%, mp 126-128 °C. $^1$H-NMR ($CDCl_3$) δ: 2.42 (s, 3H), 3.83 (s, 3H), 6.91 (d, J=9.0 Hz, 2H), 7.32 (d, J=8.6 Hz, 2H), 7.77 (d, J=9.0 Hz, 2H), 7.90 (d, J=8.6 Hz, 2H), 8.15 (s, 1H). MS (ESI): $[M]^+$=407.3, $[M+2]^+$=409.3.

*5.1.5.4. 4-Bromo-3-(4-ethoxyphenyl)-1-tosyl-1H-pyrazole (**14c**).* Following general procedure D, the crude residue purified by flash chromatography, using EtOAc:petroleum ether 1:1 (v:v) for elution, furnished **14c** as a white solid. Yield >95%, mp 104-106 °C. $^1$H-NMR ($CDCl_3$) δ: 1.42 (t, J=7.0 Hz, 3H), 2.42 (s, 3H), 4.04 (q, J=7.0 Hz, 2H), 6.89 (d, J=9.0 Hz, 2H), 7.31 (d, J=8.0 Hz, 2H), 7.76 (d, J=9.0 Hz, 2H), 7.90 (d, J=8.0 Hz, 2H), 8.14 (s, 1H). MS (ESI): $[M]^+$=421.3, $[M+2]^+$=423.3.

*5.1.6. General procedure E for the preparation of compounds **15a-r** and **16a-c**.* A stirred suspension of 4-bromo-1-(*p*-toluensulfonyl)-3-aryl-1*H*-pyrazole **13** or **14a-c** (0.5 mmol) and the appropriate phenylboronic acid (0.75 mmol) in 1,4-dioxane (6 mL containing 1 drop of water) was degassed under a stream of nitrogen over 10 min, then treated with $PdCl_2$(DPPF) (41 mg, 0.05 mmol) and CsF (190 mg, 1.25 mmol). The

reaction mixture was heated under nitrogen at 45 °C for 30 min, then at 100 °C for 18 h. The reaction mixture was cooled to room temperature, diluted with $CH_2Cl_2$ (10 mL), filtered on a pad of celite and evaporated under reduced pressure. The residue was dissolved with $CH_2Cl_2$ (15 mL), and the resultant solution was washed sequentially with water (5 mL) and brine (5 mL). The organic layer was dried and evaporated, and the residue was purified by silica gel column chromatography to give the title compound.

*5.1.6.1. 4-(Benzo[b]thiophen-2-yl)-1-tosyl-3-(3,4,5-trimethoxyphenyl)-1H-pyrazole (**15a**).* Following general procedure E, the crude residue purified by flash chromatography, using EtOAc:petroleum ether 3:7 (v:v) for elution, furnished **15a** as a yellowish oil. Yield 89%. $^1$H-NMR ($CDCl_3$) δ: 2.45 (s, 3H), 3.67 (s, 6H), 3.85 (s, 3H), 6.80 (s, 2H), 7.17 (s, 1H), 7.34 (m, 2H), 7.35 (d, J=8.4 Hz, 2H), 7.62 (m, 1H), 7.80 (m, 1H), 7.98 (d, J=8.4 Hz, 2H), 8.28 (s, 1H). MS (ESI): $[M+1]^+$=521.6.

*5.1.6.2. 4-(p-Tolyl)-1-tosyl-3-(3,4,5-trimethoxyphenyl)-1H-pyrazole (**15b**).* Following general procedure E, the crude residue purified by flash chromatography, using EtOAc:petroleum ether 2:8 (v:v) for elution, furnished **15b** as a white solid. Yield 96%, mp 163-164 °C. $^1$H-NMR ($CDCl_3$) δ: 2.34 (s, 3H), 2.43 (s, 3H), 3.65(s, 6H), 3.83 (s, 3H), 6.67 (s, 2H), 7.14 (s, 4H), 7.33 (d, J=8.2 Hz, 2H), 7.96 (d, J=8.2 Hz, 2H), 8.10 (s, 1H). MS (ESI): $[M+1]^+$=479.1.

*5.1.6.3. 4-(3-Fluoro-4-methylphenyl)-1-tosyl-3-(3,4,5-trimethoxyphenyl)-1H-pyrazole (**15c**).* Following general procedure E, the crude residue purified by flash chromatography, using EtOAc:petroleum ether 4:6 (v:v) for elution, furnished **15c** as a yellowish solid. Yield 73%, mp 76-78 °C. $^1$H-NMR ($CDCl_3$) δ: 2.26 (s, 3H), 2.43 (s,

3H), 3.67 (s, 6H), 3.80 (s, 3H), 6.66 (s, 2H), 6.91 (d, J=9.0 Hz, 1H), 7.15 (m, 2H), 7.38 (d, J=8.0 Hz, 2H), 7.96 (d, J=8,0 Hz, 2H), 8.12 (s, 1H). MS (ESI): $[M+1]^+$=497.6.

*5.1.6.4. 4-(3,4-Dimethylphenyl)-1-tosyl-3-(3,4,5-trimethoxyphenyl)-1H-pyrazole (**15d**).* Following general procedure E, the crude residue purified by flash chromatography, using EtOAc:petroleum ether 3:7 (v:v) for elution, furnished **15d** as a white solid. Yield 78%, mp 153-155 °C. $^1$H-NMR ($CDCl_3$) δ: 2.12 (s, 3H), 2.25 (s, 3H), 2.43 (s, 3H), 3.65 (s, 6H), 3.83 (s, 3H), 6.71 (s, 2H). 7.02 (dd, J=8.0 and 1.2 Hz, 1H), 7.06 (m, 2H), 7.34 (d, J=8.0 Hz, 2H), 7.96 (d, J=8.0 Hz, 2H), 8.09 (s, 1H). MS (ESI): $[M+1]^+$=493.0.

*5.1.6.5. 4-(3-Methoxy-4-methylphenyl)-1-tosyl-3-(3,4,5-trimethoxyphenyl)-1H-pyrazole (**15e**).* Following general procedure E, the crude residue purified by flash chromatography, using EtOAc:petroleum ether 3:7 (v:v) for elution, furnished **15e** as a white solid. Yield 75%, mp 65-67 °C. $^1$H-NMR ($CDCl_3$) δ: 2.18 (s, 3H), 2.44 (s, 3H), 3.66 (s, 6H), 3.68 (s, 3H), 3.82 (s, 3H), 6.67 (d, J=1.2 Hz, 1H), 6.70 (s, 2H). 6.78 (dd, J=7.6 and 1.2 Hz, 1H), 7.07 (d, J=7.6 Hz, 1H), 7.35 (d, J=7.6 Hz, 2H), 7.98 (d, J=7.6 Hz, 2H), 8.13 (s, 1H). MS (ESI): $[M+1]^+$=509.6.

*5.1.6.6. 1-Tosyl-4-(4-(trifluoromethyl)phenyl)-3-(3,4,5-trimethoxyphenyl)-1H-pyrazole (**15f**).* Following general procedure E, the crude residue purified by flash chromatography, using EtOAc:petroleum ether 3:7 (v:v) for elution, furnished **15f** as a white solid. Yield 83%, mp 72-74 °C. $^1$H-NMR ($CDCl_3$) δ: 2.44 (s, 3H), 3.65 (s, 6H), 3.83 (s, 3H), 6.59 (s, 2H), 7.36 (d, J=7.6 Hz, 2H), 7.40 (d, J=8.8 Hz, 2H), 7.58 (d, J=8.4 Hz, 2H), 7.99 (d, J=8.0 Hz, 2H), 8.20 (s, 1H). MS (ESI): $[M+1]^+$=533.0.

*5.1.6.7. 4-(4-Ethylphenyl)-1-tosyl-3-(3,4,5-trimethoxyphenyl)-1H-pyrazole (**15g**).* Following general procedure E, the crude residue purified by flash chromatography, using EtOAc:petroleum ether 2:8 (v:v) for elution, furnished **15g** as a clear oil. Yield 89%. $^{1}$H-NMR ($CDCl_3$) δ: 1.21 (t, J=7.6 Hz, 3H), 2.43 (s, 3H), 2.62 (q, J=7.6 Hz, 2H), 3.63 (s, 6H), 3.83 (s, 3H), 6.67 (s, 2H), 7.17 (s, 4H), 7.33 (d, J=8.2 Hz, 2H), 7.96 (d, J=8.0 Hz, 2H), 8.11 (s, 1H). MS (ESI): $[M+1]^+$=493.6.

*5.1.6.8. 4-(4-n-propylphenyl)-1-tosyl-3-(3,4,5-trimethoxyphenyl)-1H-pyrazole (**15h**).* Following general procedure E, the crude residue purified by flash chromatography, using EtOAc:petroleum ether 3:7 (v:v) for elution, furnished **15h** as a white solid. Yield 56%, mp 157-159 °C. $^{1}$H-NMR ($CDCl_3$) δ: 0.91 (t, J=7.2 Hz, 3H), 1.62 (m, 2H), 2.47 (s, 3H), 2.64 (q, J=7.2 Hz, 2H), 3.63 (s, 6H), 3.82 (s, 3H), 6.67 (s, 2H), 7.14 (s, 4H), 7.35 (d, J=8.0 Hz, 2H), 7.92 (d, J=8.0 Hz, 2H), 8.10 (s, 1H). MS (ESI): $[M+1]^+$=507.2.

*5.1.6.9. 4-(4-Methoxyphenyl)-1-tosyl-3-(3,4,5-trimethoxyphenyl)-1H-pyrazole (**15i**).* Following general procedure E, the crude residue purified by flash chromatography, using EtOAc:petroleum ether 3:7 (v:v) for elution, furnished **15i** as a white solid. Yield 90%, mp 136-137 °C. $^{1}$H-NMR ($CDCl_3$) δ: 2.43 (s, 3H), 3.66 (s, 6H), 3.80 (s, 3H), 3.83 (s, 3H), 6.68 (s, 2H), 6.84 (d, J=8.8 Hz, 2H), 7.16 (d, J=8.2 Hz, 2H), 7.33 (d, J=8.8 Hz, 2H), 7.96 (d, J=8.2 Hz, 2H), 8.09 (s, 1H). MS (ESI): $[M+1]^+$=495.1.

*5.1.6.10. 4-(4-(Methylthio)phenyl)-1-tosyl-3-(3,4,5-trimethoxyphenyl)-1H-pyrazole (**15j**).* Following general procedure E, the crude residue purified by flash chromatography, using EtOAc:petroleum ether 3:7 (v:v) for elution, furnished **15j** as a yellowish oil. Yield 90%. $^{1}$H-NMR ($CDCl_3$) δ: 2.43 (s, 3H), 2.47 (s, 3H), 3.66 (s, 6H),

3.84 (s, 3H), 6.66 (s, 2H), 7.10 (d, J=6.8 Hz, 2H), 7.16 (d, J=6.8 Hz, 2H), 7.38 (d, J=8.4 Hz, 2H), 7.97 (d, J=8.4 Hz, 2H), 8.12 (s, 1H). MS (ESI): $[M+1]^+$=511.1.

*5.1.6.11. 4-(3-Fluoro-4-methoxyphenyl)-1-tosyl-3-(3,4,5-trimethoxyphenyl)-1H-pyrazole (**15k**).* Following general procedure E, the crude residue purified by flash chromatography, using EtOAc:petroleum ether 4:6 (v:v) for elution, furnished **15k** as a white solid. Yield 74%, mp 165-167 °C. $^1$H-NMR ($CDCl_3$) δ: 2.43 (s, 3H), 3.68 (s, 6H), 3.80 (s, 3H), 3.84 (s, 3H), 6.66 (s, 2H), 6.84 (m, 1H), 6.91 (dd, J=8.4 and 2.0 Hz, 1H), 6.99 (d, J=2.0 Hz, 1H), 7.33 (d, J=8.4 Hz, 2H), 7.94 (d, J=8,4 Hz, 2H), 8.10 (s, 1H). MS (ESI): $[M+1]^+$=513.6.

*5.1.6.12. 4-(3-Chloro-4-methoxyphenyl)-1-tosyl-3-(3,4,5-trimethoxyphenyl)-1H-pyrazole (**15l**).* Following general procedure E, the crude residue purified by flash chromatography, using EtOAc:petroleum ether 1:1 (v:v) for elution, furnished **15l** as a white solid. Yield 88%, mp 79-81 °C. $^1$H-NMR ($CDCl_3$) δ: 2.43 (s, 3H), 3.69 (s, 6H), 3.84 (s, 3H), 3.90 (s, 3H), 6.68 (s, 2H), 6.86 (d, J=8.4 Hz, 1H), 7.08 (dd, J=8.4 and 2.0 Hz, 1H), 7.33 (d, J=2.0 Hz, 1H), 7.36 (d, J=8.4 Hz, 2H), 7.96 (d, J=8,4 Hz, 2H), 8.11 (s, 1H). MS (ESI): $[M+1]^+$=526.1.

*5.1.6.13. 4-(3-Methyl-4-methoxyphenyl)-1-tosyl-3-(3,4,5-trimethoxyphenyl)-1H-pyrazole (**15m**).* Following general procedure E, the crude residue purified by flash chromatography, using EtOAc:petroleum ether 3:7 (v:v) for elution, furnished **15m** as a white solid. Yield 90%, mp 134-136 °C. $^1$H-NMR ($CDCl_3$) δ: 2.17 (s, 3H), 2.43 (s, 3H), 3.66 (s, 6H), 3.78 (s, 3H), 3.82 (s, 3H), 6.72 (s, 2H). 6.75 (d, J=8.0 Hz, 1H), 7.02 (dd,

J=8.0 and 1.2 Hz, 1H), 7.06 (d, J=1.2 Hz, 1H), 7.33 (d, J=8.4 Hz, 2H), 7.33 (d, J=8.4 Hz, 2H), 8,07 (s, 1H). MS (ESI): $[M+1]^+$=509.6.

*5.1.6.14. 4-(4-Methoxy-3,5-dimethylphenyl)-1-tosyl-3-(3,4,5-trimethoxyphenyl)-1H-pyrazole (**15n**).* Following general procedure E, the crude residue purified by flash chromatography, using EtOAc:petroleum ether 4:6 (v:v) for elution, furnished **15n** as a white solid. Yield 73%, mp 74-76 °C. $^1$H-NMR ($CDCl_3$) δ: 2.23 (s, 6H), 2.43 (s, 3H), 3.66 (s, 6H), 3.70 (s, 3H), 3.83 (s, 3H), 6.73 (s, 2H), 6.92 (s, 2H), 7.34 (d, J=8.0 Hz, 2H), 7.96 (d, J=8.0 Hz, 2H), 8.07 (s, 1H). MS (ESI): $[M+1]^+$=523.2.

*5.1.6.15. 1-Tosyl-4-(4-(trifluoromethoxy)phenyl)-3-(3,4,5-trimethoxyphenyl)-1H-pyrazole (**15o**).* Following general procedure E, the crude residue purified by flash chromatography, using EtOAc:petroleum ether 3:7 (v:v) for elution, furnished **15o** as a clear oil. Yield 66%. $^1$H-NMR ($CDCl_3$) δ: 2.44 (s, 3H), 3.64 (s, 6H), 3.82 (s, 3H), 6.61 (s, 2H), 7.21 (d, J=8.8 Hz, 2H), 7.28 (d, J=8.8 Hz, 2H), 7.36 (d, J=8.0 Hz, 2H), 7.98 (d, J=8.0 Hz, 2H), 8.15 (s, 1H). MS (ESI): $[M+1]^+$=549.2.

*5.1.6.16. 4-(4-Ethoxyphenyl)-1-tosyl-3-(3,4,5-trimethoxyphenyl)-1H-pyrazole (**15p**).* Following general procedure E, the crude residue purified by flash chromatography, using EtOAc:petroleum ether 3:7 (v:v) for elution, furnished **15p** as a colorless oil. Yield >95%. $^1$H-NMR ($CDCl_3$) δ: 1.41 (t, J=7.0 Hz, 3H), 2.43 (s, 3H), 3.66 (s, 6H), 3.83 (s, 3H), 4.01 (q, J=7.0 Hz, 2H), 6.69 (s, 2H), 6.83 (d, J=8.8 Hz, 2H), 7.14 (d, J=8.2 Hz, 2H), 7.32 (d, J=8.2 Hz, 2H), 7.96 (d, J=8.5 Hz, 2H), 8.08 (s, 1H). MS (ESI): $[M+1]^+$=509.6.

*5.1.6.17. 4-(4-(Ethylthio)phenyl)-1-tosyl-3-(3,4,5-trimethoxyphenyl)-1H-pyrazole (**15q**).* Following general procedure E, the crude residue purified by flash chromatography, using EtOAc:petroleum ether 3:7 (v:v) for elution, furnished **15q** as a pale yellow oil. Yield 84%. $^{1}$H-NMR ($CDCl_3$) δ: 1.30 (t, J=7.4 Hz, 3H), 2.43 (s, 3H), 2.92 (q, J=7.4 Hz, 2H), 3.66 (s, 6H), 3.83 (s, 3H), 6.66 (s, 2H), 7.19 (d, J=8.2 Hz, 2H), 7.28 (d, J=8.2 Hz, 2H), 7.33 (d, J=8.4 Hz, 2H), 7.96 (d, J=8.4 Hz, 2H), 8.13 (s, 1H). MS (ESI): $[M+1]^+$=525.6.

*5.1.6.18. 4-(3-Chloro-4-ethoxyphenyl)-1-tosyl-3-(3,4,5-trimethoxyphenyl)-1H-pyrazole (**15r**).* Following general procedure E, the crude residue purified by flash chromatography, using EtOAc:petroleum ether 3:7 (v:v) for elution, furnished **15r** as a white sold. Yield >95%, mp 182-183 °C. $^{1}$H-NMR ($CDCl_3$) δ: 1.47 (t. J=7.0 Hz, 3H), 2.43 (s, 3H), 3.68 (s, 6H), 3.80 (s, 3H), 4.08 (q. J=7.0 Hz, 2H), 6.68 (s, 2H), 6.83 (d, J=8.4 Hz, 1H), 7.03 (dd, J=8.4 and 2.2 Hz, 1H), 7.31 (d, J=2.2 Hz, 1H), 7.37 (d, J=8.6 Hz, 2H), 7.95 (d, J=8,6 Hz, 2H), 8.10 (s, 1H). MS (ESI): $[M+1]^+$=544.1.

*5.1.6.19. 3-(p-Tolyl)-1-tosyl-4-(3,4,5-trimethoxyphenyl)-1H-pyrazole (**16a**).* Following general procedure E, the crude residue purified by flash chromatography, using EtOAc:petroleum ether 3:7 (v:v) for elution, furnished **16a** as a yellowish solid. Yield 79%, mp 73-75 °C. $^{1}$H-NMR ($CDCl_3$) δ: 2.17 (s, 3H), 2.34 (s, 3H), 2.43 (s, 3H), 3.69 (s, 6H), 3.89 (s, 3H), 6.42 (s, 2H), 7.02 (d, J=8.2 Hz, 2H), 7.28 (d, J=8.2 Hz, 2H), 7.36 (d, J=8.4 Hz, 2H), 7.96 (d, J=8.4 Hz, 2H), 8.13 (s, 1H). MS (ESI): $[M+1]^+$=479.6.

*5.1.6.20. 3-(4-Methoxyphenyl)-1-tosyl-4-(3,4,5-trimethoxyphenyl)-1H-pyrazole (**16b**).* Following general procedure E, the crude residue purified by flash chromatography,

using EtOAc:petroleum ether 3:7 (v:v) for elution, furnished **16b** as a white solid. Yield >95%, mp 61-63 °C. $^1$H-NMR ($CDCl_3$) δ: 2.43 (s, 3H), 3.70 (s, 6H), 3.79 (s, 3H), 3.86 (s, 3H), 6.43 (s, 2H), 6.80 (d, J=8.8 Hz, 2H), 7.33 (d, J=8.0 Hz, 2H), 7.40 (d, J=8.8 Hz, 2H), 7.96 (d, J=8.0 Hz, 2H), 8.12 (s, 1H). MS (ESI): $[M+1]^+$=495.3.

*5.1.6.21. 3-(4-Ethoxyphenyl)-1-tosyl-4-(3,4,5-trimethoxyphenyl)-1H-pyrazole (**16c**).* Following general procedure E, the crude residue purified by flash chromatography, using EtOAc:petroleum ether 2:8 (v:v) for elution, furnished **16c** as a white solid. Yield 74%, mp 62-64 °C. $^1$H-NMR ($CDCl_3$) δ: 1.39 (t, J=6.8 Hz, 3H), 2.43 (s, 3H), 3.70 (s, 6H), 3.89 (s, 3H), 4.03 (q, J=6.8 Hz, 2H), 6.43 (s, 2H), 6.79 (d, J=9.0 Hz, 2H), 7.33 (d, J=8.0 Hz, 2H), 7.38 (d, J=8.0 Hz, 2H), 7.96 (d, J=9.0 Hz, 2H), 8.12 (s, 1H). MS (ESI): $[M+1]^+$=509.3.

*5.1.7. General procedure F for the preparation of compounds **3a-r** and **4a-c**.* A stirred solution of 3,4-diaryl-1-(*p*-toluensulfonyl)-1*H*-pyrazole **15a-r** or **16a-c** (0.4 mmol) in EtOH (30 mL) was treated with aqueous NaOH 1 N (9 mL, 9 mmol, 22.5 equiv.). The mixture was stirred at 50 °C for 18 h (monitored by TLC), allowed to cool on an ice bath, the reaction mixture was treated with 1N HCl (9 mL, 9 mmol, 22.5 equiv.) and then concentrated under reduced pressure. The aqueous, concentrated mixture was diluted with a saturated aqueous solution of $NaHCO_3$ (10 mL), extracted with $CH_2Cl_2$ (2x10 mL) and the organic phase washed sequentially with water (5 mL) and brine (5 mL), dried and evaporated under reduced pressure. The residue was purified by flash chromatography on silica gel.

*5.1.7.1. 4-(Benzo[b]thiophen-2-yl)-3-(3,4,5-trimethoxyphenyl)-1H-pyrazole (**3a**).* Following general procedure F, the crude residue purified by flash chromatography, using EtOAc:petroleum ether 3:7 (v:v) for elution, furnished **3a** as a yellow solid. Yield 83%, mp 151-153 °C. $^{1}$H-NMR ($CDCl_3$) δ: 3.73 (s, 6H), 3.92 (s, 3H), 6.85 (s, 2H), 7.23 (m, 3H), 7.67 (d, J=7.4 Hz, 1H), 7.77 (d, J=7.4 Hz, 1H), 7.83 (s, 1H). $^{13}$C-NMR ($CDCl_3$) δ: 56.09 (2C), 61.00, 105.76, 106.04, 113.48, 121.47, 122.00, 123.21, 124.07, 124.44, 126.06, 134.81, 135.26, 138.55, 139.38, 140.17, 144.59, 153.35 (2C). MS (ESI): $[M+1]^+$=367.4. Anal. calcd for $C_{20}H_{18}N_2O_3S$. C, 65.55; H, 4.95; N, 7.64; found: C, 65.41; H, 4.77; N, 7.53.

*5.1.7.2. 4-(p-Tolyl)-3-(3,4,5-trimethoxyphenyl)-1H-pyrazole (**3b**).* Following general procedure F, the crude residue purified by flash chromatography, using EtOAc:petroleum ether 6:4 (v:v) for elution, furnished **3b** as a white solid. Yield 82%, mp 65-67 °C. $^{1}$H-NMR ($CDCl_3$) δ: 2.37 (s, 3H), 3.72 (s, 6H), 3.89 (s, 3H), 6.72 (s, 2H), 7.15 (d, J=7.6 Hz, 2H), 7.25 (d, J=7.6 Hz, 2H), 7.69 (s, 1H). $^{13}$C-NMR ($CDCl_3$) δ: 21.23, 56.02 (2C), 61.01, 105.17 (2C), 120.08, 126.92, 128.66 (2C), 129.23 (2C), 129.89, 134.13, 136.63, 137.96, 146.86, 153.28 (2C). MS (ESI): [M+1]+=325.2. Anal. calcd for $C_{19}H_{20}N_2O_3$. C, 70.35; H, 6.21; N, 8.64; found: C, 70.12; H, 6.06; N, 8.49.

*5.1.7.3. 4-(3-Fluoro-4-methylphenyl)-3-(3,4,5-trimethoxyphenyl)-1H-pyrazole (3c).* Following general procedure F, the crude residue purified by flash chromatography, using EtOAc:petroleum ether 9:1 (v:v) for elution, furnished **3c** as a yellow solid. Yield 65%, mp 155-157 °C. $^{1}$H-NMR ($CDCl_3$) δ: 2.29 (s, 3H), 3.71 (s, 6H), 3.89 (s, 3H), 6.71 (s, 2H), 7.00 (m, 1H), 7.03 (s, 1H), 7.12 (m, 1H), 7.67 (s, 1H). $^{13}$C-NMR ($CDCl_3$) δ: 14.28, 56.00 (2C), 60.95, 105.67 (2C), 114.83, 115.06, 118.90, 123.05, 124.00, 126.60,

132.38, 134.46, 144.19, 153.31 (2C), 160.02, 162.45. MS (ESI): $[M+1]^+$=343.0. Anal. calcd for $C_{19}H_{19}FN_2O_3$. C, 66.66; H, 5.59; N, 8.18; found: C, 66.49; H, 5.38; N, 8.07.

*5.1.7.4. 4-(3,4-Dimethylphenyl)-3-(3,4,5-trimethoxyphenyl)-1H-pyrazole (**3d**).* Following general procedure F, the crude residue purified by flash chromatography, using EtOAc:petroleum ether 7:3 (v:v) for elution, furnished **3d** as a white solid. Yield 72%, mp 136-137 °C. $^1$H-NMR ($CDCl_3$) δ: 2.23 (s, 3H), 2.28 (s, 3H), 3.68 (s, 6H), 3.88 (s, 3H), 6.76 (s, 2H), 7.08 (m, 2H), 7.16 (s, 1H), 7.66 (s, 1H). $^{13}$C-NMR ($CDCl_3$) δ: 19.42, 19.71, 55.93 (2C), 60.93, 105.23 (2C), 119.99, 126.21, 127.12, 129.67, 129.88, 130.47 134.25, 135.11, 136.54, 137.93, 143.94, 153.17 (2C). MS (ESI): $[M+1]^+$=339.4. Anal. calcd for $C_{20}H_{22}N_2O_3$. C, 70.99; H, 6.55; N, 8.28; found: C, 70.78; H, 6.44; N, 8.17.

*5.1.7.5. 4-(3-Methoxy-4-methylphenyl)-3-(3,4,5-trimethoxyphenyl)-1H-pyrazole (**3e**).* Following general procedure F, the crude residue purified by flash chromatography, using EtOAc:petroleum ether 8:2 (v:v) for elution, furnished **3e** as a pale-yellow oil. Yield 68%. $^1$H-NMR ($CDCl_3$) δ: 2.23 (s, 3H), 3.69 (s, 6H), 3.71 (s, 3H), 3.87 (s, 3H), 6.75 (s, 2H), 6.79 (d, J=2.0 Hz, 1H), 6.87 (dd, J=8.4 and 2.0 Hz, 1H), 7.09 (d, J=8.4 Hz, 1H), 7.69 (s, 1H). $^{13}$C-NMR ($CDCl_3$) δ: 15.91, 55.21, 55.98 (2C), 60.92, 105.40, 105.69, 110.51, 120.16, 120.55, 125.18, 127.08, 130.59, 131.60, 134.05, 137.98, 144.19, 153.19 (2C), 157.62. MS (ESI): $[M+1]^+$=355.1. Anal. calcd for $C_{20}H_{22}N_2O_4$. C, 67.78; H, 6.26; N, 7.90; found: C, 67.58; H, 6.15; N, 7.76.

*5.1.7.6. 4-(4-(Trifluoromethyl)phenyl)-3-(3,4,5-trimethoxyphenyl)-1H-pyrazole (**3f**).* Following general procedure F, the crude residue purified by flash chromatography,

using EtOAc:petroleum ether 6:4 (v:v) for elution, furnished **3f** as a white solid. Yield 80%, mp 159-160 °C $^{1}$H-NMR ($CDCl_3$) δ: $^{1}$H-NMR ($CDCl_3$) δ: 3.72 (s, 3H), 3.90 (s, 6H), 6.66 (s, 2H), 7.47 (d, J=8.0 Hz, 2H), 7.59 (d, J=8.0 Hz, 2H), 7.77 (s, 1H). $^{13}$C-NMR ($CDCl_3$) δ: 55.88, 60.94 (2C), 105.22 (2C), 116.67, 118.71, 121.78 (2C), 124.33, 126.45, 130.10 (2C), 131.99, 134.16, 138.20, 144.62, 148.09, 153.36 (2C). MS (ESI): $[M+1]^+$=378.9. Anal. calcd for $C_{19}H_{17}F_3N_2O_3$. C, 60.32; H, 4.53; N, 7.40; found: C, 60.13; H, 4.33; N, 7.19.

*5.1.7.7. 4-(4-Ethylphenyl)-3-(3,4,5-trimethoxyphenyl)-1H-pyrazole (**3g**).* Following general procedure F, the crude residue purified by flash chromatography, using EtOAc:petroleum ether 7:3 (v:v) for elution, furnished **3g** as a white solid. Yield 89%, mp 67-69 °C. $^{1}$H-NMR ($CDCl_3$) δ: 1.22 (t, J=7.6 Hz, 3H), 2.63 (q, J=7.6 Hz, 2H), 3.67 (s, 6H), 3.86 (s, 3H), 6.69 (s, 2H), 7.15 (d, J=8.4 Hz, 2H), 7.25 (d, J=8.4 Hz, 2H), 7.66 (s, 1H). $^{13}$C-NMR ($CDCl_3$) δ: 15.80, 28.62, 55.86 (2C), 60.95, 105.18 (2C), 119.99, 126.71, 128.02 (2C), 128.90 (2C), 130.21, 133.98, 137.86, 143.11, 144.08, 153.16 (2C). MS (ESI): $[M+1]^+$=339.0. Anal. calcd for $C_{20}H_{22}N_2O_3$. C, 70.99; H, 6.55; N, 8.28; found: C, 70.75; H, 6.38; N, 8.10.

*5.1.7.8. 4-(4-n-Propylphenyl)-3-(3,4,5-trimethoxyphenyl)-1H-pyrazole (**3h**).* Following general procedure F, the crude residue purified by flash chromatography, using EtOAc:petroleum ether 6:4 (v:v) for elution, furnished **3h** as a white solid. Yield 89%, mp 69-71 °C. $^{1}$H-NMR ($CDCl_3$) δ: 0.93 (t, J=7.4 Hz, 3H), 1.61 (m, 2H), 2.54 (t, J=7.4 Hz, 2H), 3.65 (s, 6H), 3.86 (s, 3H), 6.69 (s, 2H), 7.12 (d, J=8.0 Hz, 2H), 7.23 (d, J=8.0 Hz, 2H), 7.65 (s, 1H). $^{13}$C-NMR ($CDCl_3$) δ: 13.79, 24.68, 37.74, 55.89 (2C), 61.00,

105.08 (2C), 120.08, 127.05, 128.65 (2C), 128.78 (2C), 130.32, 133.98, 137.80, 141.44, 144.08, 153.21 (2C). MS (ESI): $[M+1]^+$=353.2. Anal. calcd for $C_{21}H_{24}N_2O_3$. C, 71.57; H, 6.86; N, 7.95; found: C, 71.38; H, 6.75; N, 7.79.

*5.1.7.9. 4-(4-Methoxyphenyl)-3-(3,4,5-trimethoxyphenyl)-1H-pyrazole (**3i**).* Following general procedure F, the crude residue purified by flash chromatography, using EtOAc:petroleum ether 1:1 (v:v) for elution, furnished **3i** as a white solid. Yield 88%, mp 88-90 °C. $^1$H-NMR ($CDCl_3$) δ: 3.67 (s, 3H), 3.83 (s, 6H), 3.88 (s, 3H), 6.72 (s, 2H), 6.87 (d, J=7.4 Hz, 2H), 7.27 (d, J=7.6 Hz, 2H), 7.65 (s, 1H). $^{13}$C-NMR ($CDCl_3$) δ: 55.40, 56.11 (2C), 61.01, 105.31 (2C), 114.09 (2C), 119.85, 124.62, 125.72, 130.09 (2C), 133.70, 138.34, 143.92, 153.38 (2C), 158.94. MS (ESI): $[M+1]^+$=341.1. Anal. calcd for $C_{19}H_{20}N_2O_4$. C, 67.05; H, 5.92; N, 8.23; found: C, 66.89; H, 5.68; N, 8.01.

*5.1.7.10. 4-(4-(Methylthio)phenyl)-3-(3,4,5-trimethoxyphenyl)-1H-pyrazole (**3j**).* Following general procedure F, the crude residue purified by flash chromatography, using EtOAc:petroleum ether 3:7 (v:v) for elution, furnished **3j** as a white solid. Yield 84%, mp 142-144 °C. $^1$H-NMR ($CDCl_3$) δ: 2.48 (s, 3H), 3.69 (s, 6H), 3.87 (s, 3H), 6.68 (s, 2H), 7.24 (m, 4H), 7.67 (s, 1H). $^{13}$C-NMR ($CDCl_3$) δ: 15.93, 56.00 (2C), 60.98, 105.31 (2C), 119.46, 126.34, 126.68 (2C), 129.09 (2C), 129.54, 134.02, 137.13, 138.11, 144.03, 153.29 (2C). MS (ESI): $[M+1]^+$=357.0. Anal. calcd for $C_{19}H_{20}N_2O_3S$. C, 64.02; H, 5.66; N, 7.86; found: C, 63.89; H, 5.49; N, 7.72.

*5.1.7.11. 4-(3-Fluoro-4-methoxyphenyl)-3-(3,4,5-trimethoxyphenyl)-1H-pyrazole (**3k**).* Following general procedure F, the crude residue purified by flash chromatography, using EtOAc:petroleum ether 9:1 (v:v) for elution, furnished **3k** as a white solid. Yield

88%, mp 172-174 °C. $^{1}$H-NMR ($CDCl_3$) δ: 3.72 (s, 6H), 3.89 (s, 3H), 3.91 (s, 3H), 6.71 (s, 2H), 6.92 (m, 1H), 7.04 (m, 1H), 7.09 (dd, J=8.0 and 2.0 Hz, 1H), 7.66 (s, 1H). $^{13}$C-NMR ($CDCl_3$) δ: 56.03, 60.95 (2C), 103.12, 105.33 (2C), 113.48, 116.24, 118.65, 124.44, 126.09, 126.62, 134.26, 138.20, 144.01, 146.46, 151.01, 153.35 (2C). MS (ESI): $[M+1]^+$=359.4. Anal. calcd for $C_{19}H_{19}FN_2O_3$. C, 63.86; H, 5.34; N, 7.82; found: C, 63.74; H, 5.21; N, 7.49.

*5.1.7.12. 4-(3-Chloro-4-methoxyphenyl)-3-(3,4,5-trimethoxyphenyl)-1H-pyrazole (**3l**).* Following general procedure F, the crude residue purified by flash chromatography, using EtOAc:petroleum ether 8:2 (v:v) for elution, furnished **3l** as a white solid. Yield 68%, mp 169-171 °C. $^{1}$H-NMR ($CDCl_3$) δ: 3.73 (s, 6H), 3.89 (s, 3H), 3.92 (s, 3H), 6.72 (s, 2H), 6.90 (d, J=8.0 Hz, 1H), 7.18 (dd, J=8.0 and 2.0 Hz, 1H), 7.42 (d, J=2.0 Hz, 1H), 7.67 (s, 1H). $^{13}$C-NMR ($CDCl_3$) δ: 56.06 (2C), 56.24, 60.96, 105.26 (2C), 112.04, 118.43, 122.37, 126.41, 126.63, 128.06, 130.24, 134.17, 138.22, 144.07, 153.36, 153.92 (2C). MS (ESI): $[M+1]^+$=375.8. Anal. calcd for $C_{19}H_{19}ClN_2O_3$. C, 60.88; H, 5.11; N, 7.47; found: C, 60.59; H, 5.03; N, 7.33.

*5.1.7.13. 4-(3-Methyl-4-methoxyphenyl)-3-(3,4,5-trimethoxyphenyl)-1H-pyrazole (**3m**).* Following general procedure F, the crude residue purified by flash chromatography, using EtOAc:petroleum ether 7:3 (v:v) for elution, furnished **3m** as a white solid. Yield 72%, mp 161-163 °C. $^{1}$H-NMR ($CDCl_3$) δ: 2.19 (s, 3H), 3.69 (s, 6H), 3.83 (s, 3H), 3.86 (s, 3H), 6.73 (s, 2H), 6.75 (d, J=8.4 Hz, 1H), 7.14 (m, 3H), 7.62 (s, 1H). $^{13}$C-NMR ($CDCl_3$) δ: 16.24, 55.46, 55.98 (2C), 61.00, 105.06 (2C), 109.92, 119.86, 124.88, 126.63, 127.17, 127.27, 131.15, 134.05, 137.82, 144.02, 153.21 (2C), 156.86. MS

(ESI): $[M+1]^+$=355.1. Anal. calcd for $C_{20}H_{22}N_2O_4$. C, 67.78; H, 6.26; N, 7.90; found: C, 67.61; H, 6.10; N, 7.72.

*5.1.7.14. 4-(4-Methoxy-3,5-dimethylphenyl)-3-(3,4,5-trimethoxyphenyl)-1H-pyrazole (**3n**).* Following general procedure F, the crude residue purified by flash chromatography, using EtOAc:petroleum ether 7:3 (v:v) for elution, furnished **3n** as a white solid. Yield 77%, mp 74-76 °C. $^1$H-NMR ($CDCl_3$) δ: 2.26 (s, 6H), 3.68 (s, 6H), 3.74 (s, 3H), 3.88 (s, 3H), 6.76 (s, 2H), 7.01 (s, 2H), 7.63 (s, 1H). $^{13}$C-NMR ($CDCl_3$) δ: 16.11 (2C), 55.93 (2C), 59.83, 61.01, 104.99 (2C), 119.75, 127.02, 128.54, 129.36 (2C), 130.88 (2C), 134.08, 137.86, 143.76, 153.19 (2C), 156.05. MS (ESI): $[M+1]^+$=369.2. Anal. calcd for $C_{21}H_{24}N_2O_4$. C, 68.46; H, 6.57; N, 7.60; found: C, 68.33; H, 6.42; N, 7.49.

*5.1.7.15. 4-(4-(Trifluoromethoxy)phenyl)-3-(3,4,5-trimethoxyphenyl)-1H-pyrazole (**3o**).* Following general procedure F, the crude residue purified by flash chromatography, using EtOAc:petroleum ether 8:2 (v:v) for elution, furnished **3o** as a white solid. Yield 67%, mp 138-140 °C. $^1$H-NMR ($CDCl_3$) δ: 3.68 (s, 3H), 3.88 (s, 6H), 6.67 (s, 2H), 7.18 (d, J=7.6 Hz, 2H), 7.38 (d, J=7.6 Hz, 2H), 7.70 (s, 1H). $^{13}$C-NMR ($CDCl_3$) δ: 56.04 (2C), 61.05, 105.34 (2C), 119.22, 121.35 (2C), 125.13, 130.35 (2C), 130.73, 131.29, 133.45, 138.62, 144.25, 148.43, 153.51 (2C). MS (ESI): $[M+1]^+$=394.8. Anal. calcd for $C_{19}H_{17}F_3N_2O_4$. C, 57.87; H, 4.35; N, 7.10; found: C, 57.69; H, 4.12; N, 6.99.

*5.1.7.16. 4-(4-Ethoxyphenyl)-3-(3,4,5-trimethoxyphenyl)-1H-pyrazole (**3p**).* Following general procedure F, the crude residue purified by flash chromatography, using EtOAc:petroleum ether 7:3 (v:v) for elution, furnished **3p** as a white solid. Yield 73%,

mp 76-77 °C. $^{1}$H-NMR ($CDCl_3$) δ: 1.39 (t, J=7.2 Hz, 3H), 3.68 (s, 6H), 3.86 (s, 3H), 4.02 (q, J=7.2 Hz, 2H), 6.70 (s, 2H), 6.85 (d, J=8.8 Hz, 2H), 7.23 (d, J=8.8 Hz, 2H), 7.63 (s, 1H). $^{13}$C-NMR ($CDCl_3$) δ: 14.83, 55.94 (2C), 60.93, 63.48, 105.02 (2C), 114.48 (2C), 119.71, 125.09, 126.93, 129.88 (2C), 133.90, 137.80, 144.02, 153.19 (2C), 157.96. MS (ESI): $[M+1]^+$=354.9. Anal. calcd for $C_{20}H_{22}N_2O_4$. C, 67.78; H, 6.26; N, 7.90; found: C, 67.58; H, 6.15; N, 7.75.

*5.1.7.17. 4-(4-(Ethylthio)phenyl)-3-(3,4,5-trimethoxyphenyl)-1H-pyrazole* ***(3q).*** Following general procedure F, the crude residue purified by flash chromatography, using EtOAc:petroleum ether 7:3 (v:v) for elution, furnished **3q** as a pale yellow solid. Yield 95%, mp 65-67 °C. $^{1}$H-NMR ($CDCl_3$) δ: 1.32 (t, J=7.6 Hz, 3H), 2.95 (q, J=7.6 Hz, 2H), 3.71 (s, 6H), 3.89 (s, 3H), 6.70 (s, 2H), 7.27 (m, 4H), 7.69 (s, 1H). $^{13}$C-NMR ($CDCl_3$) δ: 14.39, 27.73, 56.00 (2C), 61.02, 105.19 (2C), 119.47, 126.76, 129.13 (2C), 129.16 (2C), 130.53, 134.15, 135.07, 138.03, 144.09, 153.33 (2C). MS (ESI): $[M+1]^+$=370.9. Anal. calcd for $C_{20}H_{22}N_2O_3S$. C, 64.84; H, 5.99; N, 7.56; found: C, 64.72; H, 5.78; N, 7.42.

*5.1.7.18. 4-(3-Chloro-4-ethoxyphenyl)-3-(3,4,5-trimethoxyphenyl)-1H-pyrazole* ***(3r).*** Following general procedure F, the crude residue purified by flash chromatography, using EtOAc:petroleum ether 6:4 (v:v) for elution, furnished **3r** as a white solid. Yield 79%, mp 175-177 °C. $^{1}$H-NMR ($CDCl_3$) δ: 1.49 (t, J=7.2 Hz, 3H), 3.73 (s, 6H), 3.89 (s, 3H), 4.11 (q, J=7.2 Hz, 2H), 6.72 (s, 2H), 6.89 (d, J=8.4 Hz, 1H), 7.15 (dd, J=8.4 and 2,4 Hz, 1H), 7.41 (s, 1H), 7.66 (s, 1H). $^{13}$C-NMR ($CDCl_3$) δ: 14.77, 56.10 (2C), 61.04, 64.89, 105.16 (2C), 113.31, 118.57, 122.78, 126.18, 126.59, 128.08, 130.29, 132.42,

134.12, 138.15, 144.14, 153.39 (2C). MS (ESI): $[M+1]^+$=388.9. Anal. calcd for $C_{20}H_{21}ClN_2O_4$. C, 61.78; H, 5.44; N, 7.20; found: C, 61.58; H, 5.32; N, 7.09.

*5.1.7.19. 3-(p-Tolyl)-4-(3,4,5-trimethoxyphenyl)-1H-pyrazole (**4a**).* Following general procedure F, the crude residue purified by flash chromatography, using EtOAc:petroleum ether 7:3 (v:v) for elution, furnished **4a** as a pale-yellow oil. Yield 58%. $^1$H-NMR ($CDCl_3$) δ: 2.39 (s, 3H), 3.74(s, 6H), 3.988 (s, 3H), 6.54 (s, 2H), 7.17 (d, J=8.0 Hz, 2H), 7.38 (d, J=8.0 Hz, 2H), 7.70 (s, 1H). $^{13}$C-NMR ($CDCl_3$) δ: 21.30, 56.01 (2C), 60.96, 105.21 (2C), 119.67, 128.03, 128.72 (2C), 129.30 (2C), 129.55, 135.85, 136.88, 138.29, 142.84, 153.20 (2C). MS (ESI): $[M+1]^+$=325.1. Anal. calcd for $C_{19}H_{20}N_2O_3$. C, 70.35; H, 6.21; N, 8.64; found: C, 70.15; H, 6.12; N, 8.38.

*5.1.7.20. 3-(4-Methoxyphenyl)-4-(3,4,5-trimethoxyphenyl)-1H-pyrazole (**4b**).* Following general procedure F, the crude residue purified by flash chromatography, using EtOAc:petroleum ether 7:3 (v:v) for elution, furnished **4b** as a white solid. Yield 82%, mp 65-67 °C. $^1$H-NMR ($CDCl_3$) δ: 3.74 (s, 3H), 3.84 (s, 6H), 3.89 (s, 3H), 6.55 (s, 2H), 6.89 (d, J=7.4 Hz, 2H), 7.42 (d, J=7.6 Hz, 2H), 7.69 (s, 1H). $^{13}$C-NMR ($CDCl_3$) δ: 55.31, 56.02 (2C), 60.95, 105.51 (2C), 114.04 (2C), 119.44, 123.40, 128.75, 129.29 (2C), 135.70, 136.85, 142.73, 153.23 (2C), 159.73. MS (ESI): $[M+1]^+$=341.4. Anal. calcd for $C_{19}H_{20}N_2O_4$. C, 67.05; H, 5.92; N, 8.23; found: C, 66.90; H, 5.72; N, 8.10.

*5.1.7.21. 3-(4-Ethoxyphenyl)-4-(3,4,5-trimethoxyphenyl)-1H-pyrazole (**4c**).* Following general procedure F, the crude residue purified by flash chromatography, using EtOAc:petroleum ether 7:3 (v:v) for elution, furnished **4c** as a white solid. Yield 75%, mp 58-60 °C. $^1$H-NMR ($CDCl_3$) δ: 1.44 (t, J=6.8 Hz, 3H), 3.74 (s, 6H), 3.88 (s, 3H),

4.04 (q, J=6.6 Hz, 2H), 6.54 (s, 2H), 6.88 (d, J=8.8 Hz, 2H), 7.41 (d, J=8.8 Hz, 2H), 7.69 (s, 1H). $^{13}$C-NMR ($CDCl_3$) δ: 14.84, 56.05 (2C), 61.03, 63.55, 105.39 (2C), 114.59 (2C), 119.39, 123.13, 128.81, 129.63 (2C), 135.82, 136.73, 142.87, 153.23 (2C), 159.14. MS (ESI): $[M+1]^+$=355.4. Anal. calcd for $C_{20}H_{22}N_2O_4$. C, 67.78; H, 6.26; N, 7.90; found: C, 67.55; H, 6.12; N, 7.81.

*5.2. Biological assays and computational studies*

*5.2.1. Cell growth conditions and antiproliferative assay.*

Human promyelocytic leukemia (HL-60), human T-cell leukemia (CEM) and human B-cell leukemia (SEM) cells were grown in RPMI-1640 medium (Gibco, Milano, Italy). Breast adenocarcinoma (MCF-7 and MDA-MB-231), human cervix carcinoma (HeLa), and human colon adenocarcinoma (HT-29) cells were grown in DMEM medium (Gibco, Milano, Italy), all supplemented with 115 units/mL penicillin G (Gibco, Milano, Italy), 115 $\mu$g/mL streptomycin (Invitrogen, Milano, Italy), and 10% fetal bovine serum (Invitrogen, Milano, Italy). Stock solutions (10 mM) of the different compounds were obtained by dissolving them in DMSO. Individual wells of a 96-well tissue culture microtiter plate were inoculated with 100 μL of complete medium containing $8 \times 10^3$ cells. The plates were incubated at 37 °C in a humidified 5% $CO_2$ incubator overnight prior to the experiments. After medium removal, 100 μL of fresh medium containing the test compound at different concentrations was added to each well in triplicate and incubated at 37 °C for 72 h. Cell viability was assayed by the (3-(4, 5-dimethylthiazol-2-yl)-2,5-diphenyltetrazolium bromide test as previously described [47].

Normal human astrocytes were purchased from Lonza (Lonza). They were grown in AGM™ astrocytes growth Medium BullettKit™. $CEM^{Vbl\text{-}100}$ cells are a multidrug-

resistant line selected against vinblastine and were a kind gift of Dr. G. Arancia (Istituto Superiore di Sanità, Rome, Italy). They were grown in RPMI-1640 medium supplemented with 100 ng/mL of vinblastine.

Additional experiments were conducted with peripheral blood lymphocytes (PBL) from healthy donors obtained as described previously [47]. For cytotoxicity evaluations in proliferating PBL cultures, non-adherent cells were resuspended at 5 x $10^5$ cells/mL in growth medium containing 2.5 $\mu$g/mL PHA (Irvine Scientific). Different concentrations of the test compounds were added, and viability was determined 72 h later by the MTT test. For cytotoxicity evaluations in resting PBL cultures, non-adherent cells were resuspended (5 x $10^5$ cells/mL) and treated for 72 h with the test compounds, as described above.

*5.2.2. Effects on tubulin polymerization and on colchicine binding to tubulin.*

Bovine brain tubulin was purified as described previously [48]. To evaluate the effect of the compounds on tubulin assembly *in vitro* [49], varying concentrations were preincubated with 10 μM tubulin in glutamate buffer at 30 ˚C and then cooled to 0 ˚C. After addition of GTP, the mixtures were transferred to 0 °C cuvettes in a recording spectrophotometer and warmed to 30 °C, and the assembly of tubulin was observed turbidimetrically. The $IC_{50}$ was defined as the compound concentration that inhibited the extent of assembly by 50% after a 20 min incubation. Inhibition of colchicine binding to tubulin was measured as described before [50], except that the reaction mixtures contained 0.5 μM tubulin, 5 μM [$^3$H]colchicine and 5 or 0.5 μM test compound. Only one DEAE-cellulose filter was used per sample, and filtration was by gravity.

*5.2.3. Molecular modeling.*

All molecular docking studies were performed on a Viglen Genie Intel®Core™ i7-3770 vPro CPU@ 3.40 GHz x 8 running Ubuntu 16.04. Molecular Operating Environment (MOE) 2018.10 and Maestro (Schrödinger Release 2017-1) were used as molecular modeling software. The tubulin structure was downloaded from the PDB data bank (http://www.rcsb.org/; PDB code 5LYJ). The proteins were preprocessed using the Schrödinger Protein Preparation Wizard by assigning bond orders, adding hydrogens and performing a restrained energy minimization of the added hydrogens using the OPLS_2005 force field. Ligand structures were built with MOE and then prepared using the Maestro LigPrep tool by energy minimizing the structures (OPLS_2005 force field), generating possible ionization states at pH 7±2, and generating tautomers and low-energy ring conformers. After isolating a tubulin dimer structure, two 12 Å docking grids (inner-box 10 Å and outer-box 22 Å) were prepared using as centroid the co-crystallized CA-4. Molecular docking studies were performed using Glide SP precision keeping the default parameters and setting 5 as the number of output poses per input ligand to include in the solution. The output poses were saved as mol2 files. The docking results were visually inspected for their ability to bind in the active site.

Molecular dynamics simulations were performed on Supermicro Intel®Xeon® CPU ES-46200 @ 2.20 GHz x 12 running Ubuntu 14.04 using the Desmond package for MD simulation: OPLS-AA force field in explicit solvent, employing the TIP3 water model, was used. The initial coordinates for the MD simulation were taken from the best docking experiment result for each single compound. A cubic water box was used for the solvation of the system, ensuring a buffer distance of approximately 10 Å between each box side and the complex atoms. The system was neutralized adding 27 sodium counter ions. The system was minimized and pre-equilibrated using the default

relaxation routine implemented in Desmond. A 50 ns MD simulation was performed, during which the equations of motion were integrated using a 2 fs time step in the NPT ensemble, with temperature (300 K) and pressure (1 atm) constant. All other parameters were set using the Desmond default values. Data were collected every 20 ps (energy) and every 80 ps (trajectory). Each protein-ligand complex simulation was performed in triplicate, using each time a random seed as starting point. Visualization of protein-ligand complex and MD trajectory analysis were carried out using Maestro, and the RMSD analyses were performed using the Simulation Event Analysis tool of Desmond. The $\Delta G_{binding}$ values of the protein-ligand complex were calculated using the MM/GBSA method as implemented in the Prime module from Maestro using the default settings and the Maestro script termal_mmgbsa.py. Briefly, the script takes in the MD trajectory from the last 25 ns of simulation, splits it into individual frame snapshots (extracted every 0.080 ns, for a total of 313 frames), and runs each one through MMGBSA (after deleting water molecules and separating the ligand from the receptor). For each single simulation, an average $\Delta G_{binding}$ value for the 25 ns is calculated.

*5.2.4. Cell cycle analysis.*

HeLa or MDA-MB-231 cells were exposed to test compounds for 24 h. Cells were harvested by centrifugation and fixed with 70% (v/v) cold ethanol. Cells were lysed with 0.1% (v/v) Triton X-100 containing RNase A and stained with PI. A Beckman Coulter Cytomics FC500 instrument and MultiCycle for Windows software from Phoenix Flow Systems were used to analyze the cells.

*5.2.5. Measurement of apoptosis by flow cytometry.*

In these studies, the Cytomics FC500 instrument was used. The cells were stained with both PI, to stain DNA, and annexin V-fluorescein isothiocyanate, to stain membrane PS

on the cell surface (which occurs in apoptosis). The latter was done following the instructions of the manufacturer (Roche Diagnostics) of the Annexin-V-Fluos reagent.

*5.2.6. Measurement of mitochondrial membrane potential and ROS.*

Mitochondrial potential and ROS were measured in MD-MB-231 cells by flow cytometry as previously described [45], using the fluorescent dyes JC-1 and $H_2$DCFDA (Molecular Probes), respectively.

*5.2.7. Evaluation of cellular protein expression with western blots.*

Following growth for various times in the presence of **4c** or **3p**, MDA-MB-231 cells were harvested by centrifugation and washed twice in 0 °C phosphate-buffered saline (PBS). Cells were lysed with 0.1% (v/v) Triton X-100 containing RNase A at 0 °C, and supernatants were obtained by centrifuging the lysed cells at 15 000g for 10 min at 4 °C. The protein content of the solutions was measured, and 10 μg of protein from each sample was subjected to SDS-PAGE. Proteins were transferred by electroblotting to a poly(vinylidene difluoride) Hybond-P membrane from GE Healthcare. The membranes were treated with 5% bovine serum albumin in PBS containing 0.1% Tween 20 overnight at 4 °C. The membranes were then exposed for 2 h at room temperature to primary antibodies directed against cyclin B, cdc25c, cdc2 (Y15), p21, PARP, Mcl-1, XIAP (all from Cell Signaling), or GAPDH (Sigma-Aldrich; to verify equal protein loading) and subsequently for 1 h to peroxidase-labeled secondary antibodies. The membranes were visualized using ECL select (GE Healthcare), and images were acquired using an Uvitec-Alliance imaging system.

*5.2.8. Scratch-migration assay.*

Nearly confluent MDA-MB-231 cells were gently wounded through the horizontal and vertical axis using a pipette tip. Cells were washed twice to remove cell debris and then treated with **3p** or **4c** at 20 or 5 nM, respectively, for different times. Each time point image was captured at 10x magnification under a stereomicroscope. The distance between the two edges of the scratch was quantified using Image J.

*5.2.9. Evaluation of anti-tumor activity in vivo.*

Animal experiments were approved by the local animal ethics committee (OPBA, Organismo Preposto al Benessere degli Animali, Università degli Studi di Brescia, Italy) and were performed in accordance with national guidelines and regulations. Procedures involving animals and their care conformed with institutional guidelines that comply with national and international laws and policies (EEC Council Directive 86/609, OJ L 358, 12 December 1987) and with "ARRIVE" guidelines (Animals in Research Reporting In Vivo Experiments).

Seven-week-old C57BL/6 female mice were orthotopically injected into the mammary fat pad with $4 \times 10^5$ E0771 mammary carcinoma cells. When tumors were palpable, mice were randomized to control and treated groups. Treatment was performed every other day by intraperitoneal (ip) injection of **4b** (15 or 5 mg/kg), CA-4P (30 mg/kg) or vehicle (DMSO) in 100 µL final volume. Tumors were measured in vivo using a caliper: tumor volume V ($mm^3$) was calculated according to the formula $V = (D \times d^2)/2$, where D and d are the major and minor perpendicular tumor diameters in mm, respectively. Tumor volume data were analyzed with a two-way analysis of variance, and individual group comparisons were evaluated by the Bonferroni correction.

*5.2.10. Statistical analysis.*

Graphs and statistical analyses were performed using GraphPad Prism software (GraphPad, La Jolla, CA, USA). All data in graphs represented the mean of at least three independent experiments ± SEM. Statistical significance was determined using Student's t-test or ANOVA (one- or two-way) depending on the type of data. Asterisks indicate a significant difference between the treated and the control group, unless otherwise specified. * $p < 0.05$, ** $p < 0.01$, *** $p < 0.001$, **** $p < 0.0001$.

**Disclaimer**

The content of this paper is solely the responsibility of the authors and does not necessarily reflect the official views of the National Institutes of Health.

**Acknowledgment.** We wish to thank Alberto Casolari for technical assistance. AB and SF acknowledge the support of the Life Science Research Network Wales grant n$^{o}$. NRNPGSep14008, an initiative funded through the Welsh Government's Sêr Cymru program. SF is supported by the Sêr Cymru programme which is partially funded by the European regional Development Fund through the welsh Government.

**Supplementary data**. Figure S1 and $^{1}$H-NMR and $^{13}$C-NMR spectra of compounds **3a-r** and **4a-c.** Supplementary data associated with this article can be found in the online version.

**References**

[1] A. Muroyama, T. Lechler. Microtubule organization, dynamics and functions in differentiated cells. Development 144 (2017) 3012-3021.

[2] L.A. Amos. Microtubule structure and its stabilisation. Org. Biomol. Chem. 2 (2004) 2153-2160; b) C.E. Walczak. Microtubule dynamics and tubulin interacting proteins. Curr. Opin. Cell. Biol. 12 (2000) 52-56;

[3] a) N. Mahindroo, J.P. Liou, J.Y. Chang, H.P. Hsieh. Antitubulin agents for the treatment of cancer. A medicinal chemistry update. Exp. Opin. Ther. Pat. 16 (2006) 647-691; b) C. Dumontet, M. A. Jordan. Microtubule-binding agents: a dynamic field of cancer therapeutics. Nat. Rev. Drug. Discov. 9 (2010) 790-803.; c) J.A. Hadfield, S. Ducki, N. Hirst, A. McGown. T. Tubulin and microtubules as targets for anticancer drugs. Prog. Cell Cycle Res. 5 (2003) 309-325; d) R. Mikstacka, T. Stefański, J. Różański. Tubulin-interactive stilbene derivatives as anticancer agents. Cell Mol. Biol. Lett. 18 (2013) 368-397; e) F. Pellegrini, D.R. Budman. Review: tubulin function, action of antitubulin drugs, and new drug development. Cancer Invest. 23 (2005) 264-273. f) R. Alvarez, M. Medarde, R. Pelaez. New ligands of the tubulin colchicine site based on X-ray structures, Curr. Top. Med. Chem. 14 (2014) 2231-2252; g) M. J. Pérez-Pérez, E. M. Priego, O. Bueno, M. S. Martins, M. D. Canela, S. Liekens. Blocking blood flow to solid tumors by destabilizing tubulin: an approach to targeting tumor growth. J. Med. Chem. 59 (2016) 8685-8711.

[4] G.R. Pettit, S.B. Singh, E. Hamel, C.M. Lin, D.S. Alberts, D. Garcia-Kendall. Isolation and structure of the strong cell growth and tubulin inhibitor combretastatin A-4. Experentia 45 (1989) 209-211.

[5] C.M. Lin, H.H. Ho, G.R. Pettit, E. Hamel. Antimitotic natural products combretastatin A-4 and combretastatin A-2: studies on the mechanism of their inhibition of the binding of colchicine to tubulin. Biochemistry 28 (1989) 6984-6991.

[6] A.T. McGown, B.W. Fox. Differential cytotoxicity of combretastatins A1 and A4 in two daunorubucin-resistant P388 cell lines. Cancer Chemother. Pharmacol. 26 (1990) 79-81.

[7] a) K. Grosios, S.E. Holwell, A.T. McGown, G.R. Pettit, M.C. Bibby. In vivo and in vitro evaluation of combretastatin A-4 and its sodium phosphate prodrug. Br. J. Cancer 81 (1999) 1318-1327; b) L. Vincent, P. Kermani, L.M. Young, J. Cheng, F. Zhang, K. Shido, G. Lam, H. Bompais-Vincent, Z. Zhu, D.J. Hicklin, P. Bohlen, D.J. Chaplin, C. May, S. Rafii. Combretastatin A4 phosphate induces rapid regression of tumor neovessels and growth through interference with vascular endothelial-cadherin signaling. J. Clin. Invest. 115 (2005) 2992-3006; c) D.J. Chaplin, S.A. Hill. The development of combretastatin A4 phosphate as a vascular targeting agent. Int. J. Radiat. Oncol. Biol. Phys. 54 (2002) 1491-1496; d) S.L. Young, D.J. Chaplin. Combretastatin A-4 phosphate: background and current clinical status. Expert Opin. Invest. Drugs 13 (2004) 1171-1182; e) J.H. Bilenker, K.T. Flaherty, M. Rosen, L. Davis, M. Gallagher, J.P. Stevenson, W. Sun, D. Vaughn, B. Giantonio, R. Zimmer, M. Scnall, P.J. O'Dwyer. Phase I trial of combretastatin A-4 phospate with carboplatin. Clin. Cancer Res. 11 (2005) 1527-1533; f) Y. Shi. A phase I clinical trial assessing the safety and tolerability of combretastatin A4 phosphate injections. Anti-Cancer Drugs 25 (2014) 462-471.

[8] a) N.H. Nam. Combretastatin A-4 analogues as antimitotic antitumor agents. Curr. Med. Chem. 10 (2003) 1697-1722; b) A. Chaudari, S.N. Pandeya, P. Kumar, P.P. Sharma, S. Gupta, N. Soni, K.K. Verma, G. Bhardwaj, G. Combretastatin A-4 analogues as anticancer agents. Mini Rev. Med. Chem. 12 (2007) 11861205; c) G.C.Tron, T. Pirali, G. Sorba, F. Pagliai, S. Busacca, A.A.

Genazzani. Medicinal chemistry of combretastatin A4: present and future directions. J. Med. Chem. 49 (2006) 3033-3044; d) P. O. Patil, A. G. Patil, R. A. Rane, P. C. Patil, P. K. Deshmukh, S. B. Bari, D. A. Patil, S. S. Naphade. Recent advancement in discovery and development of natural product combretastatin-inspired anticancer agents. Anticancer Agents Med. Chem. 15 (2015) 955-969.; e) T. Hatanaka, K. Fujita, K. Ohsumi, R. Nakagawa, Y. Fukuda, Y. Nihei, Y. Suga, Y. Akiyama, T. Tsuji. Novel B-ring modified combretastatin analogues: synthesis and antineoplastic activity. Bioorg. Med. Chem. Lett. 8 (1998) 3371-3374.

[9] a) M. Cushman, D. Nagarathnam, D. Gopal, A.K. Chakraborti, C.M. Lin, E. Hamel. Synthesis and evaluation of stilbene and dihydrostilbene derivatives as potential anticancer agents that inhibit tubulin polymerization. J. Med. Chem. 34 (1991) 2579-2588; b) M. Cushman, D. Nagarathnam, D. Gopal, H.M. He, C.M. Lin, E. Hamel. Synthesis and evaluation of analogues of (*Z*)-1-(4-methoxyphenyl)-2-(3,4,5-trimethoxyphenyl)ethene as potential cytotoxic and antimitotic agents. J. Med. Chem. 35 (1992) 2293-2306.

[10] a) H. Rajak, P.K. Dewangan, V. Patel, D.K. Jain, A. Singh, R. Veerasamy, P.C. Sharma, A. Dixit. Design of combretastatin A-4 analogs as tubulin targeted vascular disrupting agent with special emphasis on their *cis*-restricted isomers. Curr. Pharm. Des. 19 (2013) 1923-1955; b) Y. Shan, J. Zhang, Z. Liu, M. Wang, Y. Dong. Developments of combretastatin A-4 derivatives as anticancer agents. Curr. Med. Chem. 18 (2011) 523-538; c) A. Chaudari, S.N. Pandeya, P. Kumar, P.P Sharma, S. Gupta, N. Soni, K.K. Verma, G. Bhardwaj. Combretastatin A-4 analogues as anticancer agents. Mini Rev. Med. Chem. 12 (2007) 1186-1205.

[11] K. Ohsumi, T. Hatanaka, K. Fujita, R. Nakagawa, Y. Fukuda, Y. Nihai, Y. Suga, Y. Morinaga, Y. Akiyama, T. Tsuji, T. Synthesis and antitumor activity of *cis*-restricted combretastatins 5-membered heterocyclic analogues. Bioorg. Med. Chem. Lett. 8 (1988) 3153-3158.

[12] A.B. Sanchez Maya, C. Perez-Melero, N. Salvador, R. Pelaez, E. Caballero, M. Medarde. New naphthylcombretastatins. Modifications on the ethylene bridge. Bioog. Med. Chem. 13 (2005) 2097-2107.

[13] R. Zaninetti, S.V. Cortese, S. Aprile, A. Massarotti, P.L. Canonico, G. Sorba, G. Grosa, A.A. Genazzani, T. Pirali, T. A Concise synthesis of pyrazole analogues of combretastatin A1 as potent anti-tubulin agents. ChemMedChem 8 (2013) 633-643.

[14] T. Liu, R. Cui, J. Chen, J. Zhang, Q. He, B. Yang, Y. Hu. 4,5-Diaryl-3-aminopyrazole derivatives as analogs of combretastatin A-4: synthesis and biological evaluation. Arch. Pharm. Chem. Life Sci. (2011) 279-286.

[15] D.V. Tsyganov, L.D. Konyushkin, I.B. Karmanova, S.L. Firgang, Y.A. Strelenko, M.N. Semenova, A.S. Kiselyov, V.V. Semenov. *cis*-Restricted 3-aminopyrazole analogues of combretastatins: synthesis from plant polyalkoxybenzenes and biological evaluation in the cytotoxicity and phenotypic sea urchin embryo assays. J. Nat. Prod. 76 (2013) 1485-1491.

[16] Q. Lai, Y. Wang, R. Wang, W. Lai, L. Tang, Y. Tao, Y. Liu, R. Zhang, L. Huang, H. Xiang, S. Zeng, L. Gou, H. Chen, Y. Yao, J. Yang. Design, synthesis and biological evaluation of a novel tubulin inhibitor 7a3 targeting the colchicine binding site. Eur. J. Med. Chem. 156 (2018) 162-179.

[17] A.W. Brown, M. Fisher, G.M. Tozer, C. Kanthou, J.P.A. Harrity. Sydnone cycloaddition route to pyrazole-based analogs of combretastatin A4. J. Med. Chem. 59 (2016) 9473-9488.

[18] C. Wang, S. Yang, J. Du, J. Ni, Y. Wu, J. Wang, Q. Guan, D. Zuo, K. Bao, Y. Wu, W. Zhang. Synthesis and bioevaluation of diarylpyrazoles as antiproliferative agents. Eur. J. Med. Chem. 171 (2019) 1-10.

[19] A.B.S. Maya, B. del Rey, R.P.L. de Clairac, E. Caballero, I. Barasoain, J.M. Andreu, M. Medarde. Design, synthesis and cytotoxic activities of naphthyl analogues of combretastatin A-4. Bioorg. Med. Chem. Lett. 10 (2000) 2549-2551.

[20] Among the twenty-one compounds **3a-r** and **4a-c**, five of them (**3i**, **3o-p** and **4b-c**) were recently published by Zang and co-workers in this journal as reference 18.

[21] C.M. Sun, L.G. Lin, H.J. Yu, C.Y. Cheng, Y.C. Tsai, C.W. Chu, Y.H. Din, Y.P. Chau, M.J. Don. Synthesis and cytotoxic activities of 4,5-diarylisoxazoles. Bioorg. Med. Chem. Lett. 17 (2007) 1078-1081.

[22] M. Wu, Q. Sun, C. Yang, D. Chen, J. Ding, Y. Chen, L. Lin, Y. Xie. Synthesis and activity of combretastatin A-4 analogues: 1,2,3-thiadiazoles as potent antitumor agents. Bioorg. Med. Chem. Lett. 17 (2007) 869-873.

[23] F. Bellina, S. Cauteruccio, S. Monti, R, Rossi. Novel imidazole-based combretastatin A-4 analogues: evaluation of their in vitro antitumor activity and molecular modeling study of their binding to the colchicine site of tubulin. Bioorg. Med. Chem. Lett. 16 (2006) 5757-5762.

[24] (a) R. Romagnoli, P.G. Pier Baraldi, M.D. Carrion, O. Cruz-Lopez, C. Lopez Cara, M. Tolomeo, S. Grimaudo, A. Di Cristina, M.R. Pipitone, J. Balzarini, N.

Zonta, A. Brancale, E. Hamel. Design, synthesis and structure-activity relationship of 2-(3',4',5'-trimethoxybenzoyl)-benzo[*b*]furan derivatives as a novel class of antitubulin agents. Bioorg. Med. Chem. 17 (2009) 6862-6871; b) M. Cushman, H.-M He, J.A. Katzenellenbogen, E. Hamel. Synthesis, antitubulin and antimitotic activity and cytotoxicity of analogs of 2-methoxyestradiol, an endogenous mammalian metabolite of estradiol that inhibits tubulin polymerization by binding to the colchicine. J. Med. Chem. 38 (1995) 2041-2019; c) S. Kim, S.Y. Min, S.K. Lee, W.-J. Cho. Comparative molecular field analysis study of stilbene derivatives active against A549 lung carcinoma. Chem. Pharm. Bull. 51 (2003) 516-521.

[25] M. Dupuis, M. Flego, A. Molinari, M. Cianfriglia. Saquinavir induces stable and functional expression of the multidrug transporter P-glycoprotein in human CD4 T-lymphoblastoid CEM rev cells. HIV Medicine 4 (2003) 338-345.

[26] Schrödinger Release 2017-1: Maestro, Schrödinger, LLC, New York, NY, 2017.

[27] R. Gaspari, A.E. Prota, K. Bargstem, A. Cavalli, M.O. Steinmetz. Structural basis of cis- and trans-combretastatin binding to tubulin. Chem. 2 (2017) 102-113.

[28] Schrödinger Release 2017-1: Desmond Molecular Dynamics System, D. E. Shaw Research, New York, NY, 2017. Maestro-Desmond Interoperability Tools, Schrödinger, New York, NY, 2017.

[29] F. Adasme-Carreño, C. Muñoz-Guiterrez, J. Caballero, J.H. Alzate-Morales. Performance of the MM/GBSA scoring using a binding site hydrogen bond network-based frame selection: the protein kinase case. Phys. Chem. Chem. Phys. 16, (2014) 14047-14058.

[30] Schrödinger Release 2017-1: Prime, Schrödinger, LLC, New York, NY, 2017.

[31] A.L. Blajeski, V.A. Phan, T.J. Kottke, S.H. Kaufmann. G1 and G2 cell-cycle arrest following microtubule depolymerization in human breast cancer cells. J. Clin. Invest. 110 (2002), 91-99.

[32] P.R. Clarke, L.A. Allan. Cell-cycle control in the face of damage: a matter of life or death. Trends Cell Biol. 19 (2009) 89-98.

[33] H. Kiyokawa, D. Ray. In vivo roles of cdc25 phosphatases: biological insight into the anti-cancer therapeutic targets. Anticancer Agents Med. Chem. 8 (2008) 832-836.

[34] R. Romagnoli, P.G. Baraldi, C. Lopez Cara, M. Kimatrai Salvador, R. Bortolozzi, G. Basso, G. Viola, J. Balzarini, A. Brancale, X.-H. Fu, J. Li, S.-Z. Zhang, E. Hamel. One-pot synthesis and biological evaluation of 2-pyrrolidinyl-4-amino-5-(3',4',5'-trimethoxybenzoyl) thiazole: a unique highly active antimicrotubule agent. Eur J. Med.Chem. 46 (2011) 6015-6024.

[35] R. Romagnoli, P.G. Baraldi, M. Kimatrai Salvador, D. Preti, M.A. Tabrizi, A. Brancale, X.-H. Fu, J. Li, S.-Z. Zhang., E. Hamel, R. Bortolozzi, E. Porcù, G. Basso, G. Viola. Discovery and optimization of a series of 2-aryl-4-amino-5-(3',4',5'-trimethoxybenzoyl)thiazoles as novel anticancer agents. J. Med. Chem. 55 (2012) 5433–5445

[36] R. Romagnoli, P.G. Baraldi, C. Lopez-Cara, D. Preti, M. Aghazadeh Tabrizi, J. Balzarini, M. Bassetto, A. Brancale, X.-H. Fu, Y. Gao, J. Li, S.-Z. Zhang, E. Hamel, R. Bortolozzi, G. Basso, G. Viola. Concise synthesis and biological evaluation of 2-aroyl-5-amino benzo[*b*]thiophene derivatives as a novel class of potent antimitotic agents. J. Med. Chem. 56 (2013) 9296-9309.

[37] A. Rovini, A. Savry, D. Braguer, M. Carré. Microtubule-targeted agents: when mitochondria become essential to chemotherapy. Biochim. Biophys. Acta-

Bioenerg. 1807 **(**2011) 679-688.

[38] E. Lugli, L. Troiano, A. Cossarizza, Polychromatic analysis of mitochondrial membrane potential using JC-1. Curr. Protoc. Cytom. Chapter 7 (2007) Unit7.32.

[39] N. Zamzami, P. Marchetti, M. Castedo, D. Decaudin, A. Macho, T. Hirsch, S.A. Susin, P.X. Petit, B. Mignotte, G. Kroemer. Sequential reduction of mitochondrial transmembrane potential and generation of reactive oxygen species in early programmed cell death. J. Exp. Med. 182 (1995) 367-377.

[40] J. Cai, D.P. Jones. Superoxide in apoptosis. Mitochondrial generation triggered by cytochrome c loss. J. Biol. Chem. 273 (1998) 11401–11404.

[41] H. Nohl, L. Gille, K. Staniek. Intracellular generation of reactive oxygen species by mitochondria. Biochem. Pharmacol. 69 (2005) 719-723.

[42] I.E. Wertz, S. Kusam, C. Lam, T. Okamoto, W. Sandoval, D.J. Anderson, E. Helgason, J.A. Ernst, M. Eby, J. Liu, L.D. Belmont, J.S. Kaminker, K.M. O'Rourke, K. Pujara, P. B. Kohli, A.R. Johnson, M.L. Chiu, J.R. Lill, P.K. Jackson, W.J. Fairbrother, S. Seshagiri, M.J. Ludlam, K.G. Leong, E.C. Dueber, H. Maecker, D.C. Huang, V.M. Dixit. Sensitivity to antitubulin chemotherapeutics is regulated by MCL1 and FBW7. Nature 471 (2011) 110-114.

[43] D.C. Altieri. Survivin and IAP proteins in cell-death mechanisms. Biochem. J. 430 (2010) 199-205.

[44] E. Mariotto, G. Viola, R. Ronca, Z.M. Bhujwalla, B. Accordi, V. Serafin, L. Persano, L.C. Lopez Cara, R. Bortolozzi. The novel choline kinase alpha inhibitor EB-3D induces cellular senescence, reduce tumor growth and metastatic dissemination in breast cancer. Cancers. 10 (2018) 391.

[45] For the characterization of (*E*)-3-(dimethylamino)-1-(3,4,5-trimethoxyphenyl)prop-2-en-1-one **7** see: A. Kamal, D. Dastagiri, M.J. Ramaiah, J.S. Reddy, E.V. Bharathi, M.K. Reddy, M.V.P. Sagar, T.L. Reddy, S.N.C.V.L Pushpavalli, M. Pal-Bhadra. Synthesis and apoptosis inducing ability of new anilino substituted pyrimidine sulfonamides as potential anticancer agents. Eur. J. Med. Chem. 46 (2011) 5817-5824. For the characterization of (*E*)-3-(dimethylamino)-1-(*p*-tolyl)-2-propen-1-one **8a** and (*E)*-3-(dimethylamino)-1-(4-methoxyphenyl)-2-propen-1-one **8b** see: S. Zhou, J. Wang, L. Wang, C. Song, K. Chen, J. Zhu. Enaminones as synthons for a directed C-H functionalization: RhIII-catalyzed synthesis of naphthalenes. Angew. Chem. Int. Edit. 55 (2016) 9384-9388.

[46] For the characterization of 3-(3,4,5-trimethoxyphenyl)-1*H*-pyrazole (**9**) see: L. Levi, C. Boersch, C.F. Gers, E. Merkul, T.J.J. Müller. Consecutive three-component synthesis of 3-(hetero)aryl-1*H*-pyrazoles with propynal diethylacetal as a three-carbon building block. Molecules 16 (2011) 9340-9356. For the characterization of 3-(4-tolyl)-1*H*-pyrazole (**10a**) and 3-(4-methoxyphenyl)-1*H*-pyrazole (**10b**) see: G.C. Paveglio, K. Longhi, D.N. Moreira, T.S. Munchen, A.Z. Tier, I.M. Gindri, C.R. Bender, C.P. Frizzo, N. Zanatta, H.G. Bonacorso, M.A.P. Martins. How mechanical and chemical features affect the green synthesis of 1*H*-pyrazoles in a ball mill. ACS Sustain. Chem. Eng. 2 **(**2014**)** 1895-1901.

[47] R. Romagnoli, P. G. Baraldi, C. Lopez-Cara, M. Kimatrai Salvador, D. Preti, M. Aghazadeh Tabrizi, M. Bassetto, A. Brancale, E. Hamel, I. Castagliuolo, R. Bortolozzi, G. Basso, G. Viola. Synthesis and biological evaluation of 2-

alkoxycarbonyl-3-anilino benzo[*b*]thiophenes and thieno[2,3-*b*]pyridines as new potent anticancer agents. J. Med. Chem. 56 (2013) 2606-2618.

[48] E. Hamel, C. M. Lin. Separation of active tubulin and microtubule-associated proteins by ultracentrifugation, and isolation of a component causing the formation of microtubule bundles. Biochemistry 23 (1984) 4173-4184.

[49] E. Hamel. Evaluation of antimitotic agents by quantitative comparisons of their effects on the polymerization of purified tubulin. Cell Biochem. Biophys. 38 (2003) 1-21.

[50] a) E. Hamel, C.M. Lin. Stabilization of the colchicine-binding activity of tubulin by organic acids. Biochim. Biophys. Acta 675 (1981) 226-231. b) P. Verdier-Pinard, J.-Y. Lai, H.-D. Yoo, J. Yu, B. Marquez, D. G. Nagle, M. Nambu, J. D. White, J. R. Falck, W. H. Gerwick, B. W. Day, E. Hamel. Structure-activity analysis of the interaction of curacin A, the potent colchicine site antimitotic agent, with tubulin and effects of analogs on the growth of MCF-7 breast cancer cells. Mol. Pharmacol. 53 (1998) 62-67.

Highlights

- Pyrazole-bridged CA-4 analogues modified at the 3 and 4-position were evaluated.
- The position of trimethoxyphenyl on the pyrazole was not critical for the activity.
- The results confirmed a surrogate role of 4-ethoxyphenyl group for B-ring of CA-4
- Compounds **3p** and **4c** were more active than CA-4 against a panel of cancer cells.
- Several molecules inhibited tubulin assembly with activity superior to that of CA-4.